Peridotite Melting at 1·0 and 1·5 GPa: an Experimental Evaluation of Techniques using Diamond Aggregates and Mineral Mixes for Determination of Near-solidus Melts

Article · September 1999

DOI: 10.1093/petrology/40.9.1343

CITATIONS
75

READS
51

1 author:

Trevor J. Falloon
University of Tasmania
94 PUBLICATIONS **6,079** CITATIONS

SEE PROFILE

JOURNAL OF PETROLOGY | VOLUME 40 | NUMBER 9 | PAGES 1343–1375 | 1999

Peridotite Melting at 1·0 and 1·5 GPa: an Experimental Evaluation of Techniques using Diamond Aggregates and Mineral Mixes for Determination of Near-solidus Melts

TREVOR J. FALLOON[1,2]*, DAVID H. GREEN[2], LEONID V. DANYUSHEVSKY[1] AND ULRICH H. FAUL[2]

[1]SCHOOL OF EARTH SCIENCES, UNIVERSITY OF TASMANIA, GPO BOX 252-79, HOBART, TAS. 7001, AUSTRALIA

[2]RESEARCH SCHOOL OF EARTH SCIENCES, THE AUSTRALIAN NATIONAL UNIVERSITY, CANBERRA, A.C.T. 0200, AUSTRALIA

RECEIVED JULY 6, 1998; REVISED TYPESCRIPT ACCEPTED APRIL 12, 1999

The experimental determination of liquid compositions in lherzolite as functions of pressure and temperature provides constraints on mantle dynamics and magma genesis. In this paper, we present a detailed evaluation of the use of natural mineral mixes as starting material in peridotite melting studies at 1·0 GPa. As an example we have chosen to test the data obtained by Baker & Stolper (1994, Geochimica et Cosmochimica Acta ***58,*** *2811–2827) on a lherzolite composition (MM-3) presented as a potential source for mid-ocean ridge basalts (MORB). That study is the most fully documented published melting study using natural mineral mixes. We have tested the Baker & Stolper data in three ways: (1) we have defined the liquidus phases and conditions of the partial melt compositions obtained by Baker & Stolper; (2) we have reacted these partial melt compositions with a fine-grained synthetic starting mix of MM-3 composition; (3) we have performed additional melting experiments at 1·0 and 1·5 GPa using the synthetic mix of peridotite MM-3. Our results demonstrate that only the highest temperature experiment of Baker & Stolper, performed at 1390°C, approached an equilibrium melt of peridotite MM-3 composition and that lower temperature experiments have not reached equilibrium, retaining residual unreacted minerals and metastable melt compositions. The degree of disequilibrium increases progressively with lower temperature. Disequilibrium is attributed to the lack of reaction of the natural mineral mix and to disequilibrium melting reactions of the metastable, relatively coarse-grained mineral mix. Other contributing factors include disequilibrium caused by the use of a diamond aggregate trap. We also present peridotite melting experiments using the mineral mix KLB-1 at 1·0 GPa. Our results demonstrate that the mineral mix KLB-1 fails to equilibrate even after ~340 h at temperatures of 1280–1300°C. We present reversals of the 1·0 GPa peridotite melting experiments of* Hirose & Kushiro (1993, Earth and Planetary Science Letters ***114,*** *477–489). Our reversals demonstrate that the mineral mix–diamond aggregate trap technique used by Hirose & Kushiro has also failed to produce equilibrium melts of a mantle peridotite composition. It is recommended that data from peridotite melting studies utilizing natural mineral mixes be used with reservation and that natural mineral mixes are not a suitable starting material for such studies. The use of diamond aggregate for separation and trapping of the melt phase compounds rather than solves the problems inherent in the use of natural mineral mixes.*

KEY WORDS: *anhydrous peridotite melting; sandwich experiments; natural mineral mix; diamond aggregate entrapment; batch melting; dynamic melting*

INTRODUCTION

The experimental study of melting and liquidus phase relationships in compositionally complex systems has

*Corresponding author. Telephone: 61-3-62262477. Fax: 61-3-62232547. e-mail: trevor.falloon@utas.edu.au

classically relied on determining the solidus to liquidus phase relationships of many compositions within the particular chemical system. In this way, liquidus phase volumes, cotectics and eutectic or peritectic relations have been established. In the study of the melting behaviour of the Earth's mantle, the phase relationships are complex and complementary approaches to the problem are the use of simple-system analogues, and the selection of natural magma compositions as potential primary magmas, together with model peridotite compositions as the potential mantle source. The classical approach has been to determine the liquidus phases of basaltic magmas as functions of pressure and temperature, defining those compositions and conditions for which there is a eutectic or cotectic condition, i.e. multiple saturation in olivine + orthopyroxene ± clinopyroxene ± spinel, plagioclase or garnet (Bowen, 1914; Green & Ringwood 1967; O'Hara, 1968; Myers & Johnston, 1996). The parallel melting studies of peridotite usually cannot directly determine the melt composition (because of quenching problems) but do allow estimation of melt composition and close comparison of residual phase compositions with those of liquidus phases of the basalts at the same pressures and temperatures (Jaques & Green, 1979, 1980). A most important refinement of this approach is to use a 'sandwich technique', more recently referred to as 'peridotite reaction experiments', in which the inferred melt composition for a particular P,T is placed as a layer in contact with the model source composition (Stolper, 1980; Falloon & Green, 1987). The 'sandwich' is equilibrated over an appropriate time, and mineral and glass (or fine-grained quench aggregate) are analysed by electron microprobe. The quenching problem is avoided by having a layer (large pool) of equilibrated melt (glass), in addition to the same melt composition being present throughout the 'source-layer'. In well-planned sandwich experiments, the inferred melt composition is calculated from the model source composition by mass balance calculations using an estimated melt proportion and analysed compositions of residual phases in a forward (i.e. partial melting) experiment on the model source (Falloon *et al.*, 1988; Robinson *et al.*, 1998). Thus if the calculated melt for, say, 10% melting at a particular P, T was close to, if not identical to, the actual composition of the equilibrium melt, then the sandwich experiment places a layer of 100% melt against a layer with 10% of the same melt and 90% of residual phases. The amount of chemical adjustment of the melt and residual layers to attain an equilibrium assemblage should be negligible. Melt compositions derived by this approach can be readily applied to models of 'batch melting' of mantle peridotite. Models referred to as 'batch melting' conceive adiabatic upwelling and polybaric melting but retention of the melt within the discrete upwelling mantle volume until an event of magma segregation and escape from the system. Melt compositions are defined by the bulk composition and conditions (P,T) at the depth of magma segregation. For example, the model mantle composition designated 'Hawaiian Pyrolite' (an enriched mantle composition) has been demonstrated to be a suitable source for primary intra-plate magmas, varying from olivine melilitite (produced by ~4% melting) to tholeiitic picrite (produced by ~35% melting) (Frey *et al.*, 1978) by magma segregation at pressures from ~3 GPa to 1 GPa. Temperatures of magma extraction are at or below the mantle adiabat of potential temperature ~1450°C [Green & Falloon (1998) and references therein].

Some recent approaches to magma genesis are based on continuous melt extraction by porous flow in upwelling mantle, particularly along mid-ocean ridges. The relationships between melt porosity and permeability are currently under active investigation but most models to date assume sufficient permeability for effective melt extraction at very low melt fraction (<1%) (McKenzie & Bickle, 1988; Langmuir *et al.*, 1992; Shen & Forsyth, 1995). Magmas are conceived as the product of melt pooling by focused flow within the upwelling mantle beneath mid-ocean ridges to form basaltic crust and residual lithospheric mantle. The term 'dynamic melting' is commonly applied and numerical modelling of this process attempts to derive compositions for local melts and residues which vary continuously as functions of pressure, temperature and bulk composition throughout the melting volume. Aggregation of these increments, which approach fractional melting increments, is numerically straightforward but the physical reality of melt migration, without back-reaction and re-equilibration with shallower parts of the melt volume, has not been explored. Nevertheless, arising from this emphasis on melt mobility at small melt fractions, experimental determination of compositions of low-degree (~1%) partial melts has become a focus for research.

Using the sandwich experimental approach to determine the composition of near-solidus melts is time-consuming, requiring a facility to produce multiple bulk compositions in reactive form and multiple experiments to define equilibrium mantle melts (Robinson *et al.*, 1998). However, a number of workers claim to have achieved the compositions of near-solidus melts from a single forward experiment, i.e. melting a peridotite composition at a particular P,T condition, by using porous, sintered diamond aggregates as a medium within which a small melt fraction segregates (Johnson & Kushiro, 1992; Hirose & Kushiro, 1993; Baker & Stolper, 1994; Baker *et al.*, 1995; Kushiro, 1996). For example, a recent study of anhydrous peridotite melting at 1 GPa (Baker *et al.*, 1995) using the diamond aggregate method, reported near-solidus melt compositions at 1250–1260°C. These melt compositions were siliceous, quartz normative and low in Ca/Al ratio and in normative diopside. By contrast,

earlier studies had shown near-solidus melts of fertile peridotite to be basaltic and nepheline normative. Although conclusions were challenged in unpublished and published correspondence (Falloon *et al.*, 1996), the conflicting interpretations clearly required testing. Falloon *et al.* (1997) determined liquidus temperatures and near-liquidus phase relationships for the compositions reported as partial melts at 1250 and 1260°C, 1 GPa by Baker *et al.* (1995) and also independently established the composition of liquids in equilibrium with olivine (Mg_{90}) + orthopyroxene + clinopyroxene + plagioclase at 1 GPa. Falloon *et al.* (1997) used the classical approach of exploring chemical space with bulk compositions close to multiphase saturation points, thus avoiding the quenching and small melt fraction problems. They found that for anhydrous melting of lherzolite, near-solidus melts are basaltic and are nepheline normative for fertile lherzolite (subsolidus plagioclase at 1 GPa more sodic than $An_{60}Ab_{40}$) and hypersthene + olivine normative for refractory lherzolite with high Ca/(Ca + Na) ratio (subsolidus modal plagioclase at 1 GPa more calcic than $An_{60}Ab_{40}$). Falloon *et al.* (1997) argued that results from using the sintered diamond trap were suspect and required reversal approaches in which the inferred melt composition is shown to have the same liquidus temperature and liquidus phases as deduced from the melting experiments.

Rather than discarding the diamond aggregate technique, it is desirable to attempt to understand why the method gave incorrect results, particularly as two factors, the use of diamond aggregate as a melt trap and the use of mineral mix starting materials, are possible causes of error (Falloon *et al.*, 1996). A natural mineral mix is prepared by combining naturally occurring minerals of olivine, pyroxenes, spinel ± garnet in the correct modal proportions to obtain a model upper-mantle peridotite composition (e.g. Fuji & Scarfe, 1985; Baker & Stolper, 1994) or alternatively a natural mineral mix is obtained simply by crushing a mantle xenolith (e.g. Takahashi & Kushiro, 1983; Takahashi, 1986; Hirose & Kushiro, 1993; Kushiro, 1996). In both cases the natural mineral mix is ground to an average grain size of ~30 μm. The study of Baker & Stolper (1994) is the best documented study of peridotite melting using a natural mineral mix as a starting material and the diamond aggregate as a melt trap. That study therefore provides an ideal opportunity to test the appropriateness of using diamond aggregates and natural mineral mix starting materials in mantle melting studies. In this study we extend the reversal work of Falloon *et al.* (1997) to higher melt fractions (>7%) produced at higher temperatures (>1270°C) from peridotite composition MM-3, used in the study by Baker *et al.* (1995) and Baker & Stolper (1994).

Baker & Stolper (1994) presented 'reversals' at 1310°C consisting of holding one experiment at 1290°C and a second experiment at 1330°C before bringing both experiments to a final run temperature of 1310°C (runs 44R and 43R, Baker & Stolper, 1994). Baker & Stolper (1994) were able to demonstrate that the glass compositions were within analytical uncertainty and bracketed the temperature–composition trends for each oxide for the unreversed experiments. However, the reversals were performed using diamond aggregates and the same starting material, and it is not at all certain whether the methods of Baker & Stolper (1994) simply demonstrated reproducibility of the technique as opposed to equilibrium between liquid and residual phases. Therefore, we have undertaken the following series of reversal experiments on the Baker & Stolper (1994) compositions:

(1) crystallization experiments on three of their partial melt compositions that cover the range of temperatures (1270–1390°C). The partial melt compositions chosen for study were the glass compositions reported for runs 55T, 24 and 26 [see table 2 of Baker & Stolper (1994)];

(2) peridotite melting experiments on a synthetic starting material of the peridotite composition used by Baker & Stolper (1994) (peridotite MM-3) at 1·0 and 1·5 GPa;

(3) peridotite reaction experiments using peridotite MM-3 and the partial melt compositions from runs 55T, 24 and 26 as determined by Baker & Stolper (1994).

EXPERIMENTAL AND ANALYTICAL TECHNIQUES

The starting compositions (70a-H, 73a-H, 55T-H, 24-H-2, 26-H, IE and MM-3, Table 1) were prepared from a mixture of analytical grade oxides and carbonates (Ca, Na), ground under acetone in an agate mortar. This mixture was pelletized and sintered overnight (~16–20 h) at 950°C. An appropriate amount of synthetic fayalite was then added to the sintered mix and the mixture was again ground under acetone, before storage in glass vials in a 110°C oven. The natural mineral mix powder, KLB-1, was kindly supplied by E. Takahashi. Experiments were performed using standard piston–cylinder techniques in the High Pressure Laboratory housed in the School of Earth Sciences, University of Tasmania; Research School of Earth Sciences, The Australian National University; and the Department of Geological Sciences, University of Oregon at Eugene. Experiments performed at the University of Tasmania (run numbers starting with 'T' in Tables 2 and 7) all used NaCl–Pyrex assemblies with graphite heaters, fired pyrophyllite and alumina spacers, mullite and alumina surrounds, graphite capsules and a $W_{97}Re_3/W_{75}Re_{25}$ thermocouple. The thermocouple enters the assembly through a composite two- and four-bore alumina sheath. The thermocouple was separated

Table 1: Starting compositions used in this study

Composition	Analysis	Type	SiO_2	TiO_2	Al_2O_3	Cr_2O_3	FeO	MnO	MgO	CaO	Na_2O	*mg*-no.
70a			57·3(2)	0·59(6)	19·3(2)	0·04(4)	4·2(1)		5·4(1)	6·7(1)	5·7(3)	0·696
70a-H	WDS	A(6)	57·9(2)	0·61(2)	19·28(5)	0·08(1)	4·32(5)		5·27(5)	6·90(6)	5·66(6)	0·685
73a			53·1(4)	0·62(6)	18·6(2)	0·08(6)	5·3(3)		8·5(2)	9·3(2)	4·1(3)	0·741
73a-H	WDS	A(5)	53·5(2)	0·68(4)	18·5(1)	0·09(2)	5·22(7)		8·2(1)	9·7(1)	4·0(1)	0·737
55T			50·2(2)	0·67(6)	18·1(2)	0·11(8)	6·1(2)	0·12(7)	10·5(2)	11·4(2)	2·8(2)	0·754
55T-H	EDS	A(11)	50·7(2)	0·72(5)	17·9(1)	—	6·2(1)	—	10·1(1)	11·7(1)	2·8(1)	0·744
24			50·3(3)	0·47(6)	14·7(1)	0·34(6)	6·7(2)	0·13(9)	13·1(2)	12·8(2)	1·5(2)	0·777
24-H-2	WDS	A(5)	50·5(1)	0·52(2)	14·72(5)	0·35(5)	6·67(7)	0·12(4)	12·67(9)	13·0(1)	1·46(3)	0·772
26			51·0(2)	0·35(6)	12·1(1)	0·58(6)	7·4(3)	0·17(5)	15·7(2)	11·5(2)	1·0(1)	0·791
26-H	WDS	A(5)	51·2(1)	0·39(2)	12·2(1)	0·58(6)	7·58(8)	0·18(2)	15·25(6)	11·7(1)	0·9(3)	0·782
IE			52·42	0·76	18·96		5·06		8·12	11·01	3·67	0·741
MM-3			45·50	0·11	3·98	0·68	7·18	0·13	38·30	3·57	0·31	0·905
T.L.			45·40	0·10	3·53	0·26	7·74		39·70	3·11	0·25	0·901
KLB-1			44·48	0·16	3·59	0·31	8·10	0·12	39·22	3·44	0·30	0·896
70a (98)			55·5(6)	0·61(10)	18·9(2)	0·02(2)	4·1(2)	0·08(7)	5·7(3)	6·5(2)	7·4(3)	0·712
73a (98)			52·1(5)	0·61(10)	18·0(3)	0·07(6)	5·4(3)	0·10(9)	8·8(3)	9·3(2)	4·4(2)	0·740
24 (98)			49·8(4)	0·46(8)	14·6(2)	0·28(11)	6·8(2)	0·15(8)	13·3(2)	12·6(2)	1·58(11)	0·777

Mix compositions 70a-H and 73a-H are from Falloon *et al.* (1997). WDS, wavelength-dispersive microanalysis using a Cameca SX50 microprobe housed in the Central Science Laboratory, University of Tasmania (operating conditions 15 kV, 20 ηA). EDS, energy-dispersive microanalysis using a Cameca MICROBEAM microprobe housed in the Research School of Earth Sciences, The Australian National University (operating conditions 15 kV, 5 ηA). All glass analyses have been normalized to the composition of international glass standard VG-2 (Jarosewich *et al.*, 1980), which was analysed together with the glasses under the same analytical conditions. A, analysis is an average with the number of analyses used to calculate the average given in parentheses. Numbers in parentheses next to each analysis are 1σ in terms of the last units cited; e.g. 5.22(7) represents 5·22 $\pm$ 0·07. The composition of MM-3 is that given by Baker & Stolper (1994), and the composition of KLB-1 is that reported by Hirose & Kushiro (1993). —, below detection limit during EDS microanalysis. *mg*-no., ratio Mg/(Mg + Fe), with all Fe calculated as Fe^{2+}. Glass compositions from runs 70a and 73a are from Baker *et al.* (1995), and glass compositions from runs 55T, 24 and 26 are from Baker & Stolper (1994). Peridotite T.L. is from Robinson *et al.* (1998). The compositions 70a(98), 73a(98), 24(98) are reanalysed compositions from Baker *et al.* (1995) and Baker & Stolper (1994) reported by Hirschman *et al.* (1998).

Table 2: Experimental results

No.	Run no.	*T* (°C)	Run time (h)	Composition	Phase assemblage
Peridotite melting experiments					
1 GPa					
1	T-4193	1250	240	MM-3	Ol + Opx + Cpx + Sp + Plag
2	T-4258	1275	68	MM-3	Ol + Opx + Cpx + Sp + L
3	MM3–3	1280	169	MM-3	Ol + Opx + Cpx + Sp + L
4	T-4242	1300	28	MM-3	Ol + Opx + Cpx + Sp + L
5	T-4257	1325	68	MM-3	Ol + Opx + Cpx + Sp + L
6	T-4226	1350	46	MM-3	Ol + Opx + Sp + L
7	T-4243	1400	23	MM-3	Ol + Opx + L
8	T-4330	1440	30	MM-3	Ol + Opx + L
9	T-4264	1450	27	MM-3	Ol + L
1·25 GPa					
10	T-4268	1250	73	MM-3	Ol + Opx + Cpx + Sp + Plag
1·375 GPa					
11	T-4272	1250	121	MM-3	Ol + Opx + Cpx + Sp
1·5 GPa					
12	T-4259	1250	143	MM-3	Ol + Opx + Cpx + Sp
13	T-4260	1300	143	MM-3	Ol + Opx + Cpx + Sp
14	T-4235	1350	24	MM-3	Ol + Opx + Cpx + Sp + L
15	T-4335	1425	71	MM-3	Ol + Opx + Sp + L
16	T-4263	1450	26	MM-3	Ol + Opx + L
17	T-4269	1500	31	MM-3	Ol + Opx + L
18	T-4309	1500	25	MM-3	Ol + Opx + L
19	T-4333	1525	24	MM-3	Ol + L
20	T-4326	1550	28	MM-3	Ol + L
Crystallization experiments					
55T-H					
21	T-4253	1270	54	55T-H	Plag + Cpx + Ol + L
22	T-4275	1320	23	55T-H	Cpx + L
23	T-4278	1330	18	55T-H	L
24-H-2					
24	T-4245	1330	24	24-H-2	Cpx + L
25	T-4277	1350	17	24-H-2	Cpx + L
26	T-4273	1360	6	24-H-2	L
26-H					
27	T-4244	1390	23	26-H	Opx + L
28	T-4279	1400	24	26-H	L

and protected from the graphite capsule by a 1 mm alumina disc. No pressure correction was applied to the thermocouple calibration. The thermocouple junction is formed by crossing the thermocouple wires utilizing the four-bore alumina sheath, which forms the top 5 mm of the alumina thermocouple sheath. All experimental components and starting materials were stored in a oven at 110°C. Experiments were performed using the hot piston-out technique (Johannes *et al.*, 1971), with an initial overpressurization of ~0·5 GPa at 1·0 GPa, to help

Table 2: continued

No.	Run no.	*T* (°C)	Run time (h)	Composition	Phase assemblage
Peridotite reaction experiments					
Layered					
1 GPa					
29	T-4280	1325	94	55T-H (22%)	Ol + Opx + Cpx + Sp + L
30	T-4337	1330	52	24-H-2 (21%)	Ol + Opx + Cpx + Sp + L
31	T-4256	1350	71	24-H-2 (13%)	Ol + Opx + Cpx + Sp + L
32	T-4281	1355	67	24-H-2 (35%)	Ol + Opx + Sp* + L
33	T-4255	1390	71	26-H (15%)	Ol + Opx + Sp + L
1·5 GPa					
34	T-4332	1375	98	24-H-2 (19%)	Ol + Opx + Cpx + Sp + L
35	T-4262	1400	72	26-H (14%)	Ol + Opx + Cpx + Sp + L
Mixed					
1 GPa					
36	T-4254	1270	53	55T-H (49%)	Ol + Opx + Cpx + Plag + L
37	T-4267	1275	73	IE (40%)	Ol + Opx + Cpx + Plag + L
1·5 GPa					
38	T-4293	1325	92	IE (40%)	Ol + Opx + Cpx + L
39	T-4271	1350	98	IE (40%)	Ol + Opx + Cpx + L

Ol, olivine; Opx, orthopyroxene; Cpx, clinopyroxene; Sp, spinel; Plag, plagioclase; L, glass. *Spinel which is assumed to be present but because of its low modal abundance was not found during electron microprobe microanalysis of the longitudinally cut and polished run product.

prevent oxidation of the $W_{97}Re_3/W_{75}Re_{25}$ thermocouple. Pressures are accurate to within $\pm 0{\cdot}1$ GPa. Temperature was controlled to within ± 1°C of the set point using a Eurotherm type 818 controller. A single experiment (run MM3-3, Table 2) was performed at Research School of Earth Sciences using a NaCl–Pyrex assembly, graphite heater, MgO spacers, a graphite inner capsule sealed in an outer platinum capsule and a $Pt_{70}Rh_{30}Pt_{94}Rh_6$ thermocouple entering the assembly through an alumina sheath. Experiments performed at the University of Oregon (run numbers starting with 'K' in Table 7) used a NaCl–Pyrex assembly, graphite heater, MgO spacers, a graphite capsule and a $W_{95}Re_5/W_{74}Re_{26}$ thermocouple entering the assembly through an alumina sheath. The thermocouple wires were welded under argon.

At the end of each experiment the entire experimental charge was mounted and sectioned longitudinally before polishing. Experimental run products were analysed either by wavelength-dispersive microanalysis using Cameca SX-50 microprobes housed in the Central Science Laboratory, University of Tasmania (operating conditions 15 kV, 20 ηA) or the Department of Geological Sciences, University of Oregon at Eugene (operating conditions 15 kV, 20 ηA), or energy-dispersive microanalysis using a Cameca MICROBEAM microprobe housed in the Research School of Earth Sciences, The Australian National University (operating conditions 15 kV, 5 ηA). All glass analyses have been normalized to the composition of international glass standard VG-2 (Jarosewich *et al.*, 1980), which was analysed together with the glasses under the same analytical conditions.

Our experimental results are presented in Tables 2 and 7. In Tables 3 and 8 electron microprobe analyses of selected run products and mass balance calculations are presented. The analyses presented in Tables 1, 3 and 8 have all been normalized to 100 wt % before an average was calculated. Table 3 demonstrates that our run products are essentially homogeneous and produce good mass balance with low sums of residuals squared. Our run times varied from 6 to 240 h on experiments performed using synthetic starting materials (Table 2). Run times varied according to the nature of the experiment (crystallization, reaction or melting) and temperature. Our unpublished reversal work on Falloon & Green (1987) 1 GPa glass compositions suggests that equilibrium glass compositions can be obtained within ~3 h at ~1325°C using synthetic starting materials prepared in an identical manner to those used in this study (Falloon *et al.*, in preparation).

Robinson *et al.* (1998) have also demonstrated that

Table 3: Compositions of experimental run products

Run no.	Phase	MB bulk	MB MM-3	Type	SiO_2	TiO_2	Al_2O_3	Cr_2O_3	FeO	MnO	MgO	CaO	Na_2O
Peridotite melting experiments													
T-4193	Olivine		0·55(1)	A(7)	40·8(1)			0·13(4)	9·2(1)	0·17(3)	49·5(1)	0·23(2)	
	Orthopyroxene		0·26(2)	A(3)	53·9(8)	0·25(5)	5·1(6)	0·87(5)	5·4(4)	0·15(3)	31·9(7)	2·3(2)	0·08(1)
	Clinopyroxene		0·134(7)	A(4)	51·4(2)	0·54(5)	5·9(3)	1·13(8)	3·4(2)	0·12(4)	19·1(4)	17·8(7)	0·61(3)
	Spinel		0·014(3)	A(3)		0·29(3)	51·5(9)	17·1(8)	8·9(1)		22·1(4)	0·13(2)	
	Plagioclase		0·042(9)	A(7)	54·9(6)		28·3(4)		0·47(3)		0·3(1)	11·2(5)	4·8(3)
	Residual		**0·0186**										
T-4258	Olivine			A(6)	41·1(2)			0·14(4)	8·9(1)	0·13(2)	49·5(1)	0·28(2)	
	Orthopyroxene			A(5)	54·1(5)	0·2(1)	5·8(9)	0·9(1)	5·2(2)	0·15(4)	30·9(8)	2·7(1)	0·1(1)
	Clinopyroxene			A(8)	51·7(3)	0·33(3)	6·0(3)	1·3(1)	3·5(1)	0·10(3)	19·7(7)	17·0(8)	0·42(2)
	Spinel			n.d.									
	Glass			n.d.									
MM3–3	Olivine			A(4)	41·3(1)			0·11(4)	8·8(3)		49·5(2)	0·22(8)	
	Orthopyroxene			A(3)	55·0(6)	0·11(4)	3·9(7)	1·2(2)	5·1(2)		31·8(4)	2·8(1)	
	Clinopyroxene			A(2)	51·7(4)		6·18(5)	1·5(6)	3·65(2)		19·8(2)	16·54(9)	0·3(1)
	Spinel			Sel		0·27	48·61	21·91	8·48		20·2	0·03	
	Glass			n.d.									
T-4242	Olivine			A(5)	40·90(4)			0·22(3)	8·44(4)	0·11(4)	50·00(4)	0·33(2)	
	Orthopyroxene			A(5)	55·0(6)	0·09(2)	3·6(4)	1·2(1)	4·65(9)	0·10(3)	32·59(9)	2·7(1)	0·07(0)
	Clinopyroxene			A(5)	51·9(3)	0·19(3)	5·2(3)	1·6(1)	3·4(2)	0·11(4)	20·8(6)	16·5(7)	0·32(2)
	Spinel			A(2)	0·24(1)	0·23(3)	36·59(7)	34·2(2)	8·9(3)	0·13(2)	19·6(3)	0·12(9)	
	Glass			n.d.									
T-4257	Olivine			A(9)	41·0(2)			0·24(4)	8·3(1)	0·14(5)	50·0(2)	0·31(2)	
	Orthopyroxene			A(4)	54·8(3)	0·10(1)	3·8(2)	1·31(5)	5·0(1)	0·13(2)	32·0(2)	2·8(1)	0·06(1)
	Clinopyroxene			A(5)	52·2(1)	0·2(4)	4·7(5)	1·7(1)	3·6(2)	0·10(3)	20·8(5)	16·4(3)	0·32(4)
	Spinel			A(5)	0·5(3)	0·23(2)	36(2)	34(2)	9·4(2)	0·15(3)	19·5(5)	0·11(4)	
	Glass			n.d.									
T-4226	Olivine			A(5)	40·6(1)			0·33(3)	8·0(2)	0·11(3)	50·7(1)	0·31(1)	
	Orthopyroxene			A(5)	54·7(2)	0·07(3)	3·2(1)	1·5(1)	4·97(4)	0·13(4)	32·9(2)	2·50(6)	0·05(1)
	Spinel			A(5)	0·24(6)	0·23(3)	25·8(6)	45·6(7)	10·0(1)	0·13(6)	17·82(7)	0·17(4)	
	Glass			n.d.									

Table 3: continued

Run no.	Phase	MB bulk	MB MM-3	Type	SiO_2	TiO_2	Al_2O_3	Cr_2O_3	FeO	MnO	MgO	CaO	Na_2O
T-4243	Olivine		0·592(1)	A(5)	40·83(5)			0·49(7)	7·5(1)	0·10(4)	50·8(1)	0·27(1)	
	Orthopyroxene		0·094(3)	A(3)	56·1(3)	0·03(1)	2·2(2)	1·2(2)	4·6(1)	0·09(2)	33·79(3)	2·0(2)	0·05(1)
	Glass		0·312(2)	A(3)	51·4(1)	0·49(2)	12·04(5)	0·81(1)	7·23(8)	0·16(7)	16·23(4)	10·59(7)	1·05(1)
	Residual		**0·0029**										
T-4330	Olivine		0·593(8)	A(7)	40·9(2)			0·57(7)	7·6(1)	0·13(4)	50·6(2)	0·25(1)	
	Orthopyroxene		0·06(2)	A(3)	56·5(3)	0·05(1)	2·0(1)	1·2(2)	4·8(2)	0·13(4)	33·7(2)	1·63(7)	0·04(1)
	Glass		0·34(1)	A(5)	51·6(1)	0·45(3)	10·98(4)	0·94(2)	7·64(9)	0·20(4)	17·9(1)	9·44(7)	0·84(4)
	Residual		**0·0833**										
T-4264	Olivine		0·6012(7)	A(6)	41·5(2)			0·54(2)	6·7(1)	0·11(4)	51·0(2)	0·22(1)	
	Glass		0·3970(8)	A(2)	51·72(2)	0·38(3)	10·04(5)	0·90(6)	7·99(4)	0·16(3)	19·26(8)	8·76(7)	0·79(2)
	Residual		**0·0041**										
T-4259	Olivine		0·506(4)	A(5)	40·9(1)			0·12(2)	9·1(1)	0·13(2)	49·55(6)	0·24(2)	
	Orthopyroxene		0·295(8)	A(6)	53·0(5)	0·26(3)	6·1(4)	0·78(8)	5·7(2)	0·13(3)	32·1(8)	1·8(2)	0·15(1)
	Clinopyroxene		0·178(5)	A(9)	51·4(4)	0·48(8)	6·9(5)	1·1(1)	3·7(3)	0·14(3)	19·0(7)	16·4(9)	0·93(5)
	Spinel		0·017(1)	A(3)	0·8(2)	0·28(0)	54·6(2)	13·41(1)	8·75(4)	0·16(1)	21·9(1)	0·15(7)	
	Residual		**0·0217**										
T-4260	Olivine		0·519(6)	A(7)	40·9(4)			0·14(4)	9·1(2)	0·14(3)	49·5(4)	0·28(4)	
	Orthopyroxene		0·28(1)	A(2)	53·50(2)	0·24(2)	6·2(1)	0·9(1)	5·50(9)	0·12(2)	31·34(4)	2·0(1)	0·14(1)
	Clinopyroxene		0·182(8)	A(5)	51·6(1)	0·42(4)	7·0(2)	1·16(5)	3·78(9)	0·13(5)	19·4(4)	15·8(3)	0·78(3)
	Spinel		0·018(2)	Sel	0·46	0·27	53·56	15·16	8·63	0·07	21·77	0·09	
	Residual		**0·0422**										
T-4335	Olivine		0·56(1)	A(5)	41·0(1)			0·35(3)	8·22(6)	0·14(4)	50·0(20	0·34(2)	
	Orthopyroxene		0·21(2)	A(3)	55·3(2)	0·07(2)	3·7(2)	1·55(9)	4·89(5)	0·13(3)	31·8(2)	2·6(2)	0·08(1)
	Spinel		0·01(1)	A(2)	0·21(3)	0·22(1)	30·7(4)	41·2(7)	9·65(4)	0·05(2)	18·0(3)	0·06(0)	
	Glass		0·22(2)	A(3)	49·1(1)	0·61(5)	12·8(1)	0·59(6)	7·86(9)	0·19(2)	15·49(4)	12·4(1)	0·99(5)
	Residual		**0·1082**										
T-4309	Olivine		0·571(8)	A(6)	41·1(1)			0·56(4)	7·5(2)	0·10(3)	50·48(7)	0·24(2)	
	Orthopyroxene		0·09(2)	A(4)	56·4(4)	0·04(1)	2·4(2)	1·5(2)	4·61(7)	0·08(3)	33·6(1)	1·42(7)	0·05(1)
	Glass		0·34(1)	A(3)	50·3(3)	0·46(1)	10·7(2)	0·87(3)	8·09(2)	0·15(3)	19·1(2)	9·5(1)	0·75(5)
	Residual		**0·0984**										

Run no.	Phase	MB bulk	MB MM-3	Type	SiO_2	TiO_2	Al_2O_3	Cr_2O_3	FeO	MnO	MgO	CaO	Na_2O
T-4333	Olivine		0·574(4)	A(4)	41·4(2)			0·51(2)	6·85(7)	0·13(3)	50·9(2)	0·22(2)	
	Glass		0·427(4)	Sel	50·87	0·36	9·12	0·89	8·25		21·3	8·29	0·67
	Residual		**0·094**										
T-4326	Olivine		0·543(4)	A(5)	41·2(3)			0·53(2)	6·69(7)	0·2(2)	51·2(1)	0·20(2)	
	Glass		0·458(5)	A(2)	50·3(2)	0·32(1)	8·60(4)	1·01(0)	8·31(7)	0·17(2)	22·9(3)	7·80(1)	0·62(1)
	Residual		**0·0948**										
Crystallization experiments													
T-4253	Plagioclase			A(4)	52·9(3)		29·7(2)		0·29(1)		0·14(1)	12·8(2)	4·1(1)
	Clinopyroxene			Sel	50·69	0·69	7·19	0·42	6·48	0·14	18·01	15·85	0·54
	Olivine			A(5)	39·4(2)			0·04(1)	18·0(5)	0·27(3)	42·0(4)	0·3(1)	
	Glass			n.d.									
T-4275	Clinopyroxene	–0·003(4)		A(7)	51·5(3)	0·27(4)	7·6(5)	0·8(1)	3·7(2)	–	18·5(7)	17·1(5)	0·44(3)
	Glass	1·01(1)		A(10)	50·6(4)	0·8(1)	18·3(2)	–	6·3(1)	–	9·6(1)	11·5(1)	2·8(1)
	Residual	**0·4368**											
T-4245	Clinopyroxene	0·108(6)		A(6)	52·4(4)	0·19(4)	5·3(7)	1·0(1)	3·9(2)	0·10(4)	20·6(9)	16·3(8)	0·29(4)
	Glass	0·892(7)		A(5)	50·2(2)	0·54(3)	15·8(1)	0·26(1)	7·1(1)	0·11(5)	11·6(1)	12·8(1)	1·62(1)
	Residual	**0·0543**											
T-4277	Clinopyroxene	0·008(6)		A(7)	52·9(7)	0·13(5)	4·9(9)	1·18(8)	3·76(7)		21·3(6)	15·5(3)	0·25(7)
	Glass	0·992(7)		A(10)	50·5(1)	0·55(6)	14·73(5)	0·33(3)	6·85(9)		12·55	13·08(7)	1·4(1)
	Residual	**0·0464**											
T-4244	Orthopyroxene	0·049(3)		A(3)	55·6(2)	0·06(1)	2·8(2)	1·15(6)	5·0(1)	0·13(1)	32·86(1)	2·4(1)	0·04(2)
	Glass	0·954(3)		A(3)	50·8(1)	0·44(4)	12·69(2)	0·54(5)	7·7(1)	0·21(8)	14·4(1)	12·21(9)	1·04(4)
	Residual	**0·0283**											
Peridotite reaction experiments													
Layered													
T-4280	Olivine	0·44(1)	0·579(5)	A(6)	41·23(6)			0·15(2)	8·7(1)		49·60(5)	0·30(4)	
	Orthopyroxene	0·17(2)	0·206(9)	A(5)	54·7(3)	0·09(9)	4·8(3)	1·2(2)	5·2(1)		31·3(3)	2·6(1)	
	Clinopyroxene	0·04(1)	0·080(7)	A(5)	51·7(2)	0·23(5)	6·1(2)	1·74(9)	3·6(1)		19·7(7)	16·7(8)	0·30(9)
	Spinel	0·006(3)	0·008(2)	A(9)	0·2(3)	0·22(3)	44(2)	27(2)	8·7(2)		20·2(5)	0·16(7)	
	Glass	0·33(2)	0·125(8)	A(10)	50·1(2)	0·76(4)	16·93(8)	0·20(6)	6·44(6)		11·19(9)	12·18(8)	2·15(8)
	Residual	**0·0441**	**0·0114**										

Table 3: continued

Run no.	Phase	MB bulk	MB MM-3	Type	SiO_2	TiO_2	Al_2O_3	Cr_2O_3	FeO	MnO	MgO	CaO	Na_2O
T-4337	Olivine	0·49(4)	0·62(4)	A(4)	41·0(2)			0·23(2)	9·2(2)	0·11(8)	49·2(2)	0·34(2)	
	Orthopyroxene	0·17(6)	0·21(6)	A(3)	54·3(3)	0·10(2)	4·8(2)	1·20(3)	5·5(2)	0·14(2)	31·2(1)	2·73(5)	0·06(1)
	Clinopyroxene	0·03(3)	0·04(3)	A(5)	51·9(3)	0·18(3)	5·7(2)	1·4(2)	3·9(2)	0·11(5)	20·7(6)	15·8(9)	0·33(2)
	Spinel	–0·04(5)	–0·06(4)	A(3)	0·23(3)	0·18(1)	45·2(7)	26·0(8)	8·8(2)	0·10(4)	19·4(1)	0·13(4)	
	Glass	0·32(5)	0·14(5)	A(3)	49·60(5)	0·69(4)	16·45(6)	0·23(3)	6·73(2)	0·16(0)	11·73(4)	12·68(7)	1·73(1)
	Residual	**0·5425**	**0·4779**										
T-4256	Olivine	0·501(4)	0·579(3)	A(5)	40·9(1)			0·36(8)	8·05(6)		50·2(2)	0·34(0)	
	Orthopyroxene	0·168(7)	0·193(5)	A(5)	55·2(2)	0·09(1)	3·4(3)	1·2(1)	4·9(2)	0·13(2)	32·3(2)	2·70(6)	0·05(1)
	Clinopyroxene	0·002(6)	0·002(4)	Sel	52·1	0·19	4·93	1·97	3·32	0·13	20·49	16·59	0·27
	Spinel	0·002(1)	0·0031(9)	A(5)	0·2(1)	0·24(3)	33(1)	38(1)	9·3(2)	0·12(2)	18·8(3)	0·11(7)	
	Glass	0·323(6)	0·221(4)	A(10)	50·2(1)	0·59(3)	14·6(1)	0·50(5)	6·9(1)	0·13(5)	13·2(1)	12·8(1)	1·12(3)
	Residual	**0·0102**	**0·0047**										
T-4281	Olivine	0·388(7)	0·604(6)	A(5)	41·4(1)			0·35(4)	7·9(1)		49·98(9)	0·35(5)	
	Orthopyroxene	0·08(1)	0·14(1)	A(5)	55·5(5)		3·2(4)	1·5(1)	5·1(1)		32·0(5)	2·7(1)	
	Glass	0·532(8)	0·246(7)	A(10)	50·6(1)	0·53(3)	13·8(1)	0·55(6)	6·9(1)		13·98(7)	12·46(7)	1·15(7)
	Residual	**0·0639**	**0·0433**										
T-4255	Olivine	0·504(3)	0·59(1)	A(6)	41·1(1)			0·5(1)	7·6(2)	0·12(2)	50·4(1)	0·30(3)	
	Orthopyroxene	0·097(5)	0·12(1)	A(3)	55·9(4)	0·05(1)	2·5(1)	1·3(1)	4·7(2)	0·1(1)	33·3(2)	2·2(2)	0·04(1)
	Spinel	0·001(1)	0·002(2)	A(3)	0·16(3)	0·20(1)	22·2(1)	50·1(4)	9·8(1)	0·16(1)	17·3(3)	0·1(1)	
	Glass	0·397(4)	0·29(1)	A(10)	51·0(2)	0·47(2)	12·3(1)	0·64(2)	7·4(1)	0·14(3)	15·7(1)	11·4(1)	0·94(1)
	Residual	**0·0083**	**0·0366**										
T-4332	Olivine	0·39(2)	0·51(2)	A(5)	40·4(1)			0·17(2)	9·6(2)	0·11(2)	49·3(3)	0·36(9)	
	Orthopyroxene	0·27(3)	0·31(3)	A(5)	53·1(2)	0·11(3)	6·3(3)	1·18(8)	5·6(1)	0·17(7)	30·9(1)	2·6(3)	0·10(1)
	Clinopyroxene	0·17(3)	0·16(3)	Sel	51·1	0·2	7·09	1·4	4·11	0·04	20·42	15·19	0·46
	Spinel	0·008(5)	0·013(7)	A(5)	0·26(4)	0·16(3)	52(1)	18(1)	8·6(3)	0·12(5)	20·8(3)	0·09(6)	
	Glass	0·16(3)	0·01(4)	A(7)	48·1(2)	0·92(1)	16·24(6)	0·22(4)	7·62(5)	0·16(5)	12·9(2)	12·17(8)	1·71(9)
	Residual	**0·1047**	**0·1715**										
T-4262	Olivine	0·446(5)	0·53(1)	A(10)	41·1(2)			0·27(4)	8·42(9)	0·15(3)	49·7(2)	0·32(2)	
	Orthopyroxene	0·272(9)	0·28(2)	A(5)	54·9(3)		4·4(3)	1·41(4)	5·14(6)		31·5(1)	2·76(5)	
	Clinopyroxene	0·0007(1)	0·0008(2)	Sel	51·57	0·12	6·42	1·71	3·76		20·56	15·43	0·44
	Spinel	0·001(1)	0·005(2)	A(5)		0·21(5)	43(1)	28(1)	8·7(1)		20·1(2)	0·14(5)	
	Glass	0·268(6)	0·17(1)	A(8)	48·4(1)	0·65(3)	14·4(1)	0·38(2)	7·7(1)	0·15(3)	14·45(4)	12·6(1)	1·25(4)
	Residual	**0·0066**	**0·0328**										

Run no.	Phase	MB bulk	MB MM-3	Type	SiO_2	TiO_2	Al_2O_3	Cr_2O_3	FeO	MnO	MgO	CaO	Na_2O
Mixed													
T-4254	Olivine			A(5)	40·21(8)			0·13(2)	12·1(1)		47·1(2)	0·34(3)	
	Orthopyroxene			A(5)	53·2(2)	0·28(1)	6·0(7)	0·79(7)	6·8(2)	0·15(4)	30·2(3)	2·5(2)	0·10(1)
	Clinopyroxene			Sel	51·51	0·57	6·41	0·98	4·31	0·13	18·47	17·08	0·56
	Plagioclase			A(3)	53·3(3)		28·7(3)		0·6(2)		1·0(5)	12·4(4)	4·13(7)
	Glass*			Sel	50·86	1·37	18·57	0·06	7·39	0·23	7·87	9·62	4·04
T-4267	Olivine			A(4)	41·1(1)				10·75(8)		47·67(8)	0·28(2)	
	Orthopyroxene			A(4)	53·5(3)	0·25(3)	6·6(4)	0·9(2)	5·41(8)	0·16(6)	30·8(7)	2·41(9)	
	Clinopyroxene			A(7)	51·6(3)	0·42(9)	7·3(2)	1·2(1)	3·7(3)		18·4(4)	17·0(6)	0·46(3)
	Plagioclase			A(4)	54·1(2)		28·9(2)		0·21(4)		0·01(1)	12·0(2)	4·8(2)
	Glass*			A(9)	51·3(5)	1·7(1)	18·7(3)	0·10(6)	6·3(1)		7·8(2)	9·5(1)	4·5(1)
T-4293	Olivine	0·25(3)	0·59(3)	A(5)	41·0(1)			0·01(3)	9·74(6)		49·0(1)	0·31(4)	
	Orthopyroxene	0·24(5)	0·22(6)	A(7)	53·7(2)	0·14(7)	6·8(3)	0·8(1)	5·5(1)		30·4(1)	2·5(2)	
	Clinopyroxene	0·10(3)	0·13(4)	Sel	51·84	0·25	7·19	0·82	3·7		19	16·41	0·8
	Glass	0·40(3)	0·06(4)	A(9)	49·1(2)	1·08(3)	18·1(2)		6·9(2)		10·6(4)	10·3(1)	3·8(1)
	Residual	**0·6016**	**0·8511**										
T-4271	Olivine	0·24(2)	0·57(2)	A(6)	41·24(8)			0·10(2)	9·15(8)		49·20(8)	0·30(3)	
	Orthopyroxene	0·25(4)	0·21(3)	A(5)	53·3(6)	0·16(4)	7·5(4)	0·76(8)	5·4(1)		30·6(7)	2·3(2)	
	Clinopyroxene	0·11(3)	0·15(2)	Sel	51·64	0·38	8·16	0·75	3·97		19·66	14·85	0·66
	Glass	0·40(3)	0·05(2)	A(10)	48·9(2)	0·98(4)	17·5(1)	0·11(2)	7·0(1)		11·5(1)	10·57(7)	3·4(1)
	Residual	**0·3133**	**0·1818**										

Numbers in parentheses next to each analysis or mass balance are 1σ in terms of the last units cited. Mass balance in weight fraction was performed using least-squares linear regression using the software PETMIX and 'Residual' refers to the square of the sum of the residuals. 'MB bulk' refers to mass balance using the bulk composition of the experiment whereas 'MB MM-3' refers to mass balance using the peridotite composition MM-3 only. Analyses for runs T-4267, T-4271, T-4275, T-4277, T-4280, T-4281 and T-4293 were obtained using EDS analysis; all others are WDS (operating conditions as described for Table 1). 'Type' refers to whether the analysis given is an average (A) with the number used to form the average given in parentheses; a selected analysis (Sel) in those cases (commonly clinopyroxene) where either the small size of the crystal or its form (e.g. thin tabular laths) caused analyses to have significant overlaps with other phases. n.d., not determined, either because the glass phase was quench modified or because the very small grain size (especially spinel) made analysis without significant overlaps impossible. *Glass composition is the least modified by quench crystallization. All analyses have been normalized to 100 wt % before averages have been calculated.

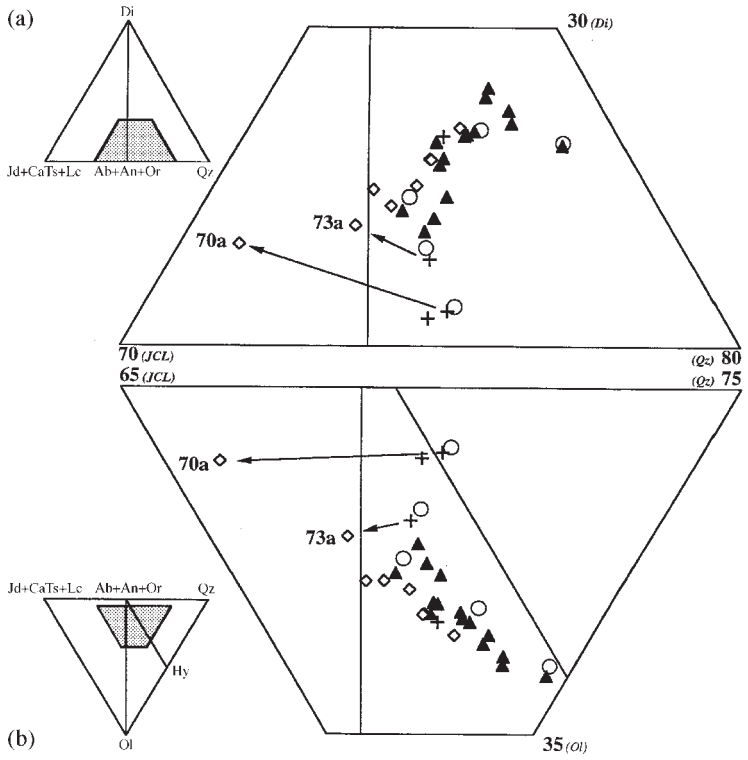

Fig. 1. Molecular normative projection from olivine (a) onto the face [Jd + CaTs + Lc]–Di–Qz and from diopside (b) onto the base [Jd + CaTs + Lc]–Qz–Ol of the 'basalt tetrahedron' (Falloon & Green, 1988; see insert) displaying the comparison between the glass compositions of Baker & Stolper (1994), Baker *et al.* (1995) and Hirschmann *et al.* (1998) with our starting mixes (Table 1). ▲, Baker & Stolper (1994); + , Baker *et al.* (1995); ◇, Hirschmann *et al.* (1998); ○; starting compositions, this study. Arrows show the shift in composition for the Baker *et al.* (1995) runs 70a and 73a (see text).

equilibrium peridotite melt compositions at 1·5 GPa utilizing the 'sandwich' approach and synthetic starting materials can be obtained during 42–50 h for peridotite reaction experiments at temperatures between 1267 and 1336°C. Our run times at 1·5 GPa for peridotite reaction experiments vary from 72 to 98 h at temperatures between 1325 and 1400°C (Table 2). Our run times for peridotite reaction experiments at 1 GPa vary from 52 to 94 h at temperatures between 1270 and 1390°C (Table 2). Therefore we believe that our experimental run times are sufficient to have produced experimental run products closely matching equilibrium assemblages for the respective bulk compositions used.

Starting compositions

In Table 1 the starting compositions used in this study are compared with those determined by Baker & Stolper (1994) and Baker *et al.* (1995), and the close matching of compositions is illustrated in Fig. 1. Our mixes fall within the compositional spectrum of those workers' glass compositions and individual oxides also match extremely well (Table 1).

Also listed in Table 1 and plotted in Fig. 1 are the reanalysed Baker & Stolper (1994) and Baker *et al.* (1995) compositions reported in an appendix by Hirschmann *et al.* (1998).

Falloon *et al.* (1997) demonstrated that the published glass compositions at 1250 and 1260°C of Baker *et al.* (1995) were not equilibrium melts. The new analysis of the 1250°C composition reported by Hirschmann *et al.* (1998) (70a, Table 1 and Fig. 1) has ~2 wt % less SiO_2 and ~2 wt % more Na_2O than originally reported (Table 1). The reanalysed compositions are now nepheline normative (vs quartz normative) (Fig. 1), in agreement with the conclusions of Falloon *et al.* (1996, 1997), but the validity of either the revised or original glass compositions as equilibrium melts should be confirmed.

Temperature control and H_2O content of experimental glasses

Using the Fourier transform IR (FTIR) technique of Danyushevsky *et al.* (1993), we have determined the H_2O contents of glasses in eight representative crystallization

and layered reaction experiments, performed using synthetic starting materials and our experimental techniques at 1 GPa. H_2O contents range from 0·07 to 0·17 wt % with an average of 0·11 ± 0·03; the accuracy of the technique is ~±0·03 wt %.

Because of inherent difficulties in interlaboratory comparisons using different thermocouples (Holloway & Wood, 1988), furnace assemblies and possible water contents, it is desirable to have an independent means of comparing temperatures obtained between different laboratories. Falloon & Danyushevsky (1999) demonstrated that the olivine geothermometer of Ford *et al.* (1983) can calculate the olivine liquidus temperatures of anhydrous basaltic to andesitic melts with <3 wt % total alkalis and in equilibrium with olivine at temperatures from 1150 to 1650°C and at pressures from 1 atm to 3·5 GPa, to within experimental uncertainty (~±15°C). Figure 2 demonstrates that glass compositions presented in this study at 1·0 and 1·5 GPa (Tables 3 and 8), with <3 wt % Na_2O in equilibrium with olivine, have calculated anhydrous olivine liquidus temperatures, mostly within ~±10°C, and all within ±15°C of the actual run temperatures using the Ford *et al.* (1983) olivine geothermometer. In this study we use the Ford *et al.* (1983) olivine geothermometer as a 'tool' to evaluate relative temperature differences between experimental data sets, including the possible effects of dissolved H_2O. If the melt is not anhydrous, then the calculated liquidus temperature using the Ford *et al.* (1983) geothermometer will be higher than the true run temperature, because of the liquidus depression caused by dissolved H_2O in the melt. In the experiments presented in this study we do not detect any effect caused by the very small amounts of H_2O present in our experiments (see above) and we therefore believe that our experiments closely approximate anhydrous conditions for melt compositions in equilibrium with olivine, as demonstrated by Fig. 2.

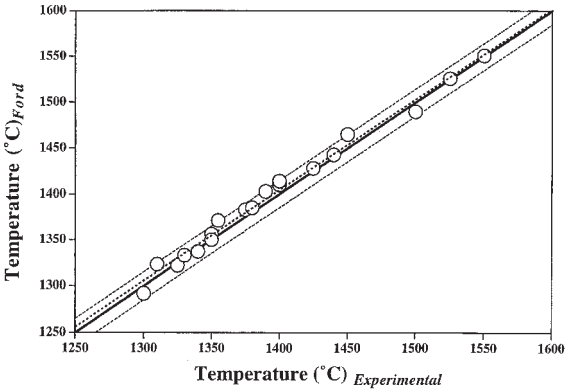

Fig. 2. Experimental run temperatures vs calculated temperatures using the olivine geothermometer of Ford *et al.* (1983). ○, experimental data from Table 3 with <3 wt % Na_2O in equilibrium with olivine at 1·0 and 1·5 GPa. Bold continuous line is a 1:1 line; fine dashed lines represent ±15°C from the 1:1 line. Bold dashed line represents the best linear fit through all our data.

CRYSTALLIZATION EXPERIMENTS

Rationale of crystallization experiments

The rationale of the crystallization experiments is based on the fact that if a melt composition is in equilibrium with a residual phase assemblage at a certain P and T, then it should be possible to demonstrate that the liquidus of the melt composition lies at this stated P and T, within experimental uncertainty (±15°C).

The melt composition should also be multiply saturated in all the residual phases. This means that if we add a few percent of one or all of the residual phases at the stated P and T to the melt composition, then the residual phases should remain stable (although they may change their compositions slightly) and the composition of the re-equilibrated melt and mineral phases should be the same as in the original experiment.

We emphasize that a test for multiple saturation of a particular melt composition does not involve a demonstration of crystallization of a peridotitic residual phase assemblage at some temperature below its liquidus. Rather, the sandwich approach is the test of whether the melt remains unchanged in composition when placed in reaction relation with the source peridotite, at the appropriate P and T.

Mix 26-H (run 26, 1390°C liquid)

The experiments reported by Baker & Stolper (1994) and Baker *et al.* (1995) were either first- or second-stage experiments (Baker & Stolper, 1994). In first-stage diamond aggregate experiments, the glass composition reported is that trapped in the diamond aggregate after holding the mineral mix MM-3 and the diamond aggregate trap for a specific amount of time and then quenching the experiment. In second-stage experiments, the MM-3 mineral mix is first held at P,T without a diamond aggregate trap and after a certain length of time the experiment is quenched. The reacted MM-3 mineral mix, now consisting of crystals + glass, is extracted from this first-stage experiment and rerun in a new second-stage experiment with a diamond aggregate trap. This is believed to produce a better approach to equilibrium compared with first-stage diamond aggregate experiments especially at lower temperatures (<1300°C). The melt composition from run 26 (Baker & Stolper, 1994) was the result of a first-stage diamond aggregate experiment at 1390°C, run for ~48 h, producing a residual spinel harzburgite assemblage.

Table 4: Glass and liquidus phases determined for mix 26-H vs run 26

	Orthopyroxene		Glass	
	Run 26 A(5)	T-4244 A(3)	Run 26 A(11)	T-4244 A(3)
SiO_2	55·2(3)	55·6(2)	51·0(2)	50·8(1)
TiO_2	0·01(1)	0·06(1)	0·35(6)	0·44(4)
Al_2O_3	2·69(13)	2·8(2)	12·1(1)	12·69(2)
Cr_2O_3	1·42(13)	1·15(6)	0·58(6)	0·54(5)
FeO	4·96(12)	5·0(1)	7·4(3)	7·7(1)
MnO	0·12(2)	0·13(1)	0·17(5)	0·21(8)
MgO	33·99(14)	32·86(1)	15·7(2)	14·4(1)
CaO	1·94(4)	2·4(1)	11·5(2)	12·21(9)
Na_2O	0·05(1)	0·04(2)	1·0(1)	1·04(4)
mg-no.	92·43	92·13	79·08	76·92

Run 26 data from Baker & Stolper (1994). Other details as for Tables 1 and 3.

Crystallization experiments on mix 26-H (Table 1) are presented in Table 2. At 1400°C mix 26-H is above its liquidus and at 1390°C, mix 26-H crystallized ~5% orthopyroxene (run T-4244, Tables 2 and 3). Where, with increasing pressure, liquidus olivine is replaced by clinopyroxene or orthopyroxene, the extrapolated olivine liquidus temperature will lie below the pyroxene liquidus. The results are consistent within experimental uncertainty with the calculated olivine liquidus of run 26 of 1405°C using the Ford *et al.* (1983) geothermometer. Both orthopyroxene and glass compositions in run T-4244 and run 26 (Baker & Stolper, 1994) are similar (Table 4) so that the reversal experiment T-4244 is in agreement, within the limits of reproducibility of P,T between laboratories, with the forward experiment. For this, the highest temperature experiment of the earlier study, there is good interlaboratory agreement in temperature and pressure measurement, and in analytical methods.

Mix 24-H-2 (run 24, 1330°C liquid)

The melt composition from run 24 was the result of a first-stage diamond aggregate experiment at 1330°C, run for ~72 h, producing a residual spinel lherzolite assemblage. Crystallization experiments on mix 24-H-2 (Table 1) are presented in Table 2. The liquidus of mix 24-H-2 lies between 1350 and 1360°C, which compares well with a calculated anhydrous olivine liquidus temperature of 1356°C using the Ford *et al.* (1983) geothermometer. At 1330°C (run T-4245, Table 2), the stated P and T of run 24, mix 24-H-2 crystallized ~11% clinopyroxene. The crystallization experiments suggest that run 24 of Baker & Stolper (1994) is not an anhydrous equilibrium melt of peridotite MM-3 at 1330°C at 1 GPa.

Mix 55T-H (run 55T, 1270°C liquid)

The melt composition from run 55T was the result of a two-stage diamond aggregate experiment at 1270°C. The first stage consisted of running peridotite MM-3 for 120 h without a diamond aggregate trap, and the second stage involved running the quenched MM-3 mineral mix from the first-stage experiment for a further 31·6 h with a diamond aggregate (Baker & Stolper, 1994). Mix 55T-H (Table 1) at the stated P and T (1270°C) of run 55T, produced a highly crystalline run product consisting of plagioclase ($An_{63·3}$), clinopyroxene (*mg*-number = 83·2) and olivine (*mg*-number = 80·6) (run T-4253, Tables 2 and 3). The anhydrous liquidus (clinopyroxene) for mix 55T-H lies between 1320 and 1330°C (runs T-4275 and T-4278, Tables 2 and 3), ~50–60°C higher than the stated run temperature of run 55T. The Ford *et al.* (1983) geothermometer calculates an anhydrous olivine liquidus temperature of 1316°C, which is lower than the experimentally determined liquidus and is consistent with another phase being on the liquidus. The crystallization experiments strongly suggest that the melt composition of run 55T is not an equilibrium melt of peridotite MM-3 at 1270°C under 'nominally anhydrous' conditions.

Melt compositions at 1250°C and 1260°C (Baker *et al.*, 1995)

Falloon *et al.* (1997) showed that anhydrous liquidus temperatures and liquidus phases of the Baker *et al.* (1995) melts at 1250 and 1260°C were inconsistent with the original melting experiments. Liquidus temperatures at 1 GPa were ~1310°C and ~1315°C, respectively.

Summary

From an above-liquidus and near-liquidus experiment, it is possible to infer liquidus temperatures for the five compositions studied and compare these with the actual run temperature in the Baker & Stolper (1994) and Baker *et al.* (1995) experiments. Inferred and actual run temperature agree only at the highest temperature (1390°C). With decreasing temperature, there is a roughly linear increase in the difference between stated and determined liquidus temperatures, rising to $\Delta T = 60$°C for the 1250°C Baker *et al.* experiment.

An explanation for the trend observed is increasing amounts of water in the analysed glasses of Baker & Stolper (1994) and Baker *et al.* (1995) at progressively lower temperatures. Based on the results of Falloon & Danyushevsky (1999) only ~0·5 wt % H_2O is necessary to cause a liquidus depression of ~60°C in the compositions of Baker & Stolper (1994) and Baker *et al.* (1995) at 1250°C. It is interesting to note that this amount of H_2O present in the 1250°C experiment of Baker *et al.* (1995) is consistent with the reported water content of 0·4 ± 0·1 wt % H_2O by Hirschmann *et al.* (1998).

REACTION EXPERIMENTS

Rationale of peridotite reaction experiments

We have two reasons for performing peridotite reaction experiments:

(1) to determine the composition of the 'anhydrous' partial melt compositions appropriate for peridotite MM-3;

(2) the crystallization experiments on the partial melt compositions of Baker & Stolper (1994) and Baker *et al.* (1995) demonstrate that apart from run 26, none of those workers' compositions examined are liquids at their stated P and T, and either their melt compositions are not equilibrium melts or contain small amounts ($\leq$0·5 wt %, Hirschmann *et al.*, 1998) of dissolved H_2O in the melt. To test the possibility that the Baker & Stolper (1994) and Baker *et al.* (1995) compositions represent equilibrium melts with small amounts of dissolved H_2O we have performed peridotite reaction experiments at the temperatures of their peridotite melting experiments (Table 2). The synthetic mix compositions should melt and remain unchanged at the end of the experiment and match very closely the glass composition in the original experiment. This will also be true of the residual mineral phases, which should be identical to those in the original experiment. The effect of up to 0·5% H_2O in the lowest temperature (1250–1260°C) experiments is predictably very small in terms of shift of phase boundaries and is negligible in the higher temperature experiments.

Mix 26-H

In run T-4255 (Tables 2 and 3) a layer of mix 26-H (15 wt %) was reacted with a layer of peridotite MM-3 (85 wt %) at 1390°C for 71 h. The experiment resulted in a spinel harzburgite residue in equilibrium with ~40 wt % melt (Table 3). As can be seen from Table 5 and Fig. 3, the glass and residual phases from run T-4255 are an excellent match to the glass and residual phases in run 26 of Baker & Stolper (1994) and Baker *et al.* (1995). This result provides convincing evidence that run 26 does indeed represent an equilibrium melt of peridotite MM-3 as we have significantly changed the modal abundances of equilibrium phases, hence the bulk composition, yet have not changed the compositions of coexisting phases.

Mix 24-H-2

In run T-4281 (Tables 2 and 3) a layer of mix 24-H-2 (35 wt %) was reacted with a layer of peridotite MM-3 (65 wt %) at 1355°C, the determined liquidus of run 24, for 67 h. The experiment resulted in a harzburgite residue in equilibrium with ~53 wt % melt (Table 3). As can be seen from Tables 1 and 3, and Fig. 3, the glass from run T-4281 is significantly different from the glass in run 24. This result strongly suggests that the run 24 is not an equilibrium melt of peridotite MM-3 at 1330°C, 1 GPa.

To help define the composition of anhydrous liquids appropriate for the MM-3 composition we have performed two additional reaction experiments using mix 24-H-2. In run T-4256 (Tables 2 and 3) a layer of mix 24-H-2 (13 wt %) was reacted with a layer of peridotite MM-3 at 1350°C for 71 h. The experiment resulted in a spinel lherzolite residue in equilibrium with ~32 wt % melt. In run T-4337 (Tables 2 and 3) a layer of mix 24-H-2 (21 wt %) was reacted with a layer of peridotite MM-3 at 1330°C for 52 h. The experiment resulted in a moderately crystalline (cpx + glass) layer overlying a spinel lherzolite residue in the peridotite layer. It was only possible to analyse pools of melt at the top part of the glass layer. The average of three glasses which we believe have not suffered any significant quench modification are presented in Table 3.

Tables 1 and 3 and Fig. 3 demonstrate that there are significant differences between the compositions of glass in our peridotite reaction experiments compared with run 24. Figure 3 demonstrates that run 24 has higher normative diopside (Fig. 3a) and higher normative [Jd + CaTs + Lc] at a given normative olivine (Fig. 3b) than the composition of glasses in our peridotite reaction experiments.

Mix 55T-H

In run T-4280 a layer of mix 55T-H (22 wt %) was reacted with a layer of peridotite MM-3 at 1325°C, the determined liquidus of run 55T, for 94 h. This resulted in a spinel lherzolite residue with a glass composition showing significant differences from the glass in run 55-T (Tables 1 and 3 and Fig. 3). This result strongly suggests that the run 55T is not an equilibrium melt of peridotite MM-3 at 1270°C, 1 GPa.

Table 5: Phase compositions from run T-4255 and run 26

	Olivines		Orthopyroxenes		Spinels		Glasses	
	T-4255 A(6)	26 A(7)	T-4255 A(3)	26 A(5)	T-4255 A(3)	26 A(4)	T-4255 A(10)	26 A(11)
SiO_2	41·1(1)	40·7(2)	55·9(4)	55·2(3)	0·16(3)	0·42(4)	51·0(2)	51·0(2)
TiO_2			0·05(1)	0·01(1)	0·20(1)	0·15(3)	0·47(2)	0·35(6)
Al_2O_3		0·06(1)	2·5(1)	2·69(13)	22·2(1)	23·3(3)	12·3(1)	12·1(1)
Cr_2O_3	0·5(1)	0·37(4)	1·3(1)	1·42(13)	50·1(4)	49·1(8)	0.64(2)	0·58(6)
FeO	7·6(2)	7·90(11)	4·7(2)	4·96(12)	9·8(1)	10·20(6)	7·4(1)	7·4(3)
MnO	0·12(2)	0·14(4)	0·1(1)	0·12(2)	0·16(1)	0·18(3)	0·14(3)	0·17(5)
MgO	50·4(1)	51·6(3)	33·3(2)	33·99(14)	17·3(3)	18·2(2)	15·7(1)	15·7(2)
CaO	0·30(3)	0·28(2)	2·2(2)	1·94(4)	0·1(1)	0·07(7)	11·4(1)	11·5(2)
Na_2O			0·04(1)	0·05(1)			0·94(1)	1·0(1)
mg-no.	92·2	92·1	92·7	92·4	75·9	76	79·1	79·1
Mode (wt %)	50·4(3)	51·1(1·2)	9·7(5)	17·2(1·3)	0·1(1)	0·26(11)	39·7(4)	27·4(1·0)

Run 26 data from Baker & Stolper (1994). Other details as for Tables 1 and 3.

To define the composition of an anhydrous liquid in equilibrium with MM-3 at 1270°C we performed a peridotite reaction experiment using mix 55T-H. In run T-4254, 49 wt % of mix 55T-H was intimately mixed and reacted with peridotite MM-3 at 1270°C for 53 h. This resulted in a highly crystalline assemblage with a plagioclase lherzolite residue. However, it was not possible to obtain analyses of glass free from the effects of quench modification. In Table 3 we present the least modified glass analysis from run T-4254 (Fig. 3). This composition is very close to other melt compositions in equilibrium with plagioclase lherzolite (Kinzler & Grove, 1992; Soulard & Wood, 1994; Walter & Presnall, 1994; Falloon *et al.*, 1997; P. Nimis *et al.*, unpublished data, 1997).

PERIDOTITE MELTING EXPERIMENTS

1 GPa melting experiments

Peridotite melting experiments on MM-3 are presented in Table 2 and residual phase compositions are presented in Table 3. Our new experimental results confirm the experimental results of Falloon *et al.* (1997) demonstrating that MM-3 is subsolidus at 1250°C at 1 GPa with a plagioclase-bearing spinel lherzolite assemblage, and our new experimental results demonstrate that the solidus lies between 1250 and 1275°C at 1 GPa. We have performed additional experiments at 1250°C at 1·25 and 1·375 GPa (runs T-4268 and T-4272, Table 2) demonstrating that plagioclase disappears as a subsolidus phase in the MM-3 composition at ~1·3 GPa. Our results show that clinopyroxene is eliminated from the residue close to 1350°C at 1 GPa and that orthopyroxene is eliminated from the residue between 1440 and 1450°C at 1 GPa (Table 2).

In high-degree ($\geq$31 wt %) melting experiments at $\geq$1400°C it was possible to obtain many consistent glass analyses that appear to be free from the effects of quench modification, as a result of the presence of relatively large glass pools. We were able to obtain very good mass balances with very low residual sums (0·003–0·08, Table 3).

1·5 GPa melting experiments

Peridotite melting experiments at 1·5 GPa are presented in Tables 2 and 3. The solidus for MM-3 lies between 1300 and 1350°C, clinopyroxene is eliminated from the residue between 1350 and 1425°C, and orthopyroxene is eliminated from the residue between 1500 and 1525°C. As it was only possible to analyse glass free from the effects of quench modification in the higher temperature experiments $\geq$1425°C, additional reaction experiments were performed at 1325, 1350, 1375 and 1400°C (Tables 2 and 3) to define the position of the 1·5 GPa melting cotectic, appropriate for peridotite of MM-3 composition, in the normative basalt tetrahedron.

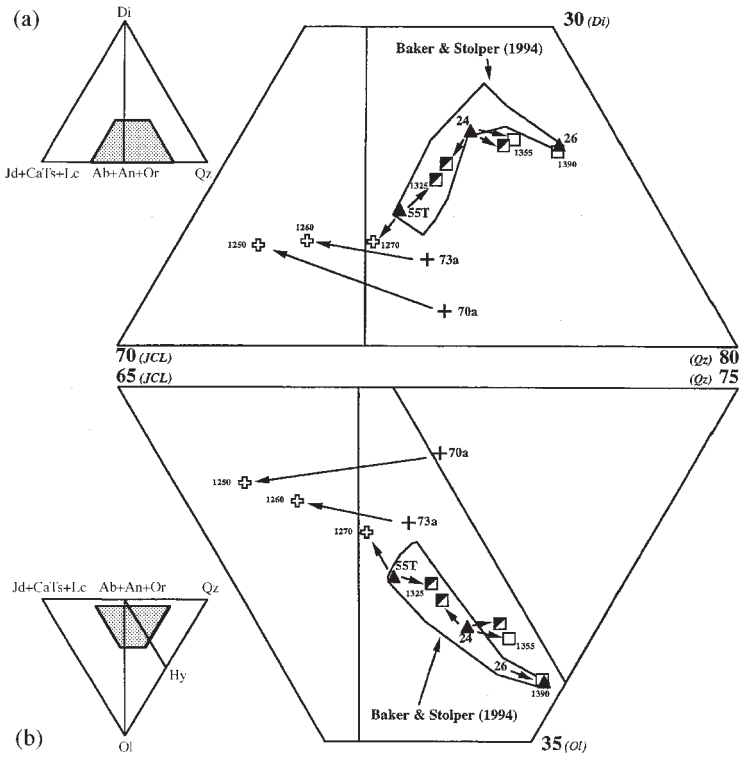

Fig. 3. Molecular normative projection from Olivine (a) onto the face [Jd + CaTs + Lc]–Di–Qz and from Diopside (b) onto the base [Jd + CaTs + Lc]–Qz–Ol of the 'basalt tetrahedron' showing glasses in our layered and mixed peridotite reaction experiments compared with the compositions of runs 55T, 24 and 26 (filled triangles) of Baker & Stolper (1994). Open field encloses all the glass compositions of Baker & Stolper (1994). Diagonally filled squares are glasses in layered peridotite reaction experiments which resulted in a spinel lherzolite residue, and open squares are glasses in layered peridotite reaction experiments which resulted in a spinel harzburgite residue. Open crosses are mixed reaction experiments which resulted in a plagioclase lherzolite residue. Filled crosses are the 1250°C (70a) and 1260°C (73a) glass compositions from Baker *et al.* (1995) and lines connect these compositions to the mixed reaction experiments of Falloon *et al.* (1997) performed at the same temperatures (open crosses).

DISCUSSION

Near-solidus melt compositions of MM-3 at 1·0 and 1·5 GPa

Our peridotite reaction experiments allow us to define the compositions of near-solidus melts of MM-3 peridotite compositions at both 1·0 and 1·5 GPa (Table 6). At 1 GPa the subsolidus assemblage is a plagioclase-bearing spinel lherzolite. As Falloon *et al.* (1997) have discussed, the composition of the subsolidus phases is critical in determining the composition of the near-solidus melt composition. The composition of the subsolidus plagioclase for the MM-3 bulk composition is therefore a very important constraint on the composition of the near-solidus melt. Falloon *et al.* (1997) determined that the subsolidus plagioclase for MM-3 at 1250°C had a composition of ~An_{68}. On the basis of this experimental result we have used our higher temperature glass data to calculate (by linear regression of oxides against temperature) a liquid composition to approximate to that in equilibrium with olivine of *mg*-number 90·5 and plagioclase An_{68}. This composition, called IE (for Initial

Table 6: Near-solidus melts for peridotite MM-3

Pressure (GPa):	1·0	1·5
Temperature (°C):	1260	1325
Residue:	Pl + Sp lherzolite	Sp lherzolite
SiO_2	52·57	49·21
TiO_2	1·44	1·08
Al_2O_3	18·77	18·16
FeO	5·07	6·62
MgO	8·14	10·79
CaO	8·72	10·32
Na_2O	5·16	3·81
mg-no.	74·10	74·40

Equilibrium melt), is presented in Table 1. A synthetic starting material of this composition was prepared and, in run T-4267 (Tables 2 and 3), 40 wt % of the IE composition was mixed with 60 wt % of the MM-3 composition and run at 1275°C (15°C above the inferred solidus temperature of 1260°C) for 73 h. Our rationale was to react the IE composition with MM-3 at a temperature above its inferred liquidus to obtain an equilibrium melt composition, close to the solidus in equilibrium with a spinel lherzolite residue. The composition of the resultant glass would then be used as a reactant in a peridotite reaction experiment at a lower temperature closer to the solidus. Run T-4267, however, resulted in a largely crystalline run product in which only very small glass pools remained, together with a plagioclase lherzolite residue. The plagioclase has a composition of An_{58}. The average of the least quench modified glass compositions is presented in Table 3, and plotted in Fig. 4. This result combined with the mixed reaction experiment T-4254 and those of Falloon *et al.* (1997) define the compositions of liquids in equilibrium with plagioclase-bearing lherzolites, similar to the peridotite composition MM-3 but differing in the composition of their subsolidus plagioclase ($An_{41–63}$) and solidus temperature (1250–1270°C; with uncertainty of $\pm$15°C). The glasses from these reaction experiments are plotted in the normative tetrahedron and compared with glass compositions determined at higher temperatures in equilibrium with spinel lherzolite (Fig. 4). The projection from olivine (Fig. 4a) shows that the trend of near-solidus melt compositions at 1 GPa is towards compositions that have low normative Di and are nepheline normative for lower temperature and more sodic plagioclase. The glass in equilibrium with An_{63} (run T-4254) is hypersthene normative. The more extensive data set suggests that the determination of An_{68} as the composition of subsolidus plagioclase on MM-3 composition (Falloon *et al.*, 1997) is in error. We performed an additional experiment on MM-3 at 1250°C for 240 h (run T-4193, Tables 2 and 3). Run T-4193 confirmed our earlier conclusion that the MM-3 composition is subsolidus at 1250°C but the plagioclase composition is significantly more sodic (~An_{56}, Table 3) than the plagioclase analysed in the 55 h experiment of Falloon *et al.* (1997). We attribute the earlier result to overlap between plagioclase and clinopyroxene analyses or to failure to achieve equilibrium with plagioclase and clinopyroxene. Using the more consistent result from run T-4193 we have calculated (by interpolation in a linear regression of oxides vs plagioclase compositions) a near-solidus melt in equilibrium with plagioclase of An_{56} and olivine of *mg*-number 90·5 using the data from the mixed reaction experiments that resulted in a plagioclase lherzolite residue. This composition is presented in Table 6 and plotted in Fig. 4. The near-solidus melt composition at 1 GPa for MM-3, which is relatively refractory in terms of Na_2O and TiO_2 contents among the spectrum of lherzolites modelled as possible mantle source compositions, is nepheline normative.

To define the composition of near-solidus peridotite melts at 1·5 GPa we used the IE composition in mixed reaction experiments with peridotite MM-3 at 1325 and 1350°C (runs T-4293 and T-4271, Tables 2 and 3). Run T-4293 (1325°C) and run 4271 (1350°C) produced lherzolite residues with large melt pools such that it was possible to obtain analyses of glass free from the effects of quench modification. The glass compositions are nepheline normative (Fig. 5) and lie on the extension of the trend defined by higher temperature glass compositions from layered experiments on MM-3 (4262, 4332). Significantly, the pyroxenes in equilibrium with the glass from run T-4293 (Table 3) are similar in composition to those analysed in the subsolidus run at 1300°C (T-4260, Tables 2 and 3). We therefore believe that the glass in run T-4293 has a composition very close to the initial melt of MM-3 composition at 1·5 GPa. The glass in run T-4293 is also very similar to that determined by Robinson *et al.* (1998) at 1325°C for the peridotite composition T.L. (Table 1, Fig. 5). The small difference apparent in the projection from olivine (Fig. 5a) reflects the slightly more refractory nature of TL when compared with MM-3 in terms of jadeite content of near-solidus pyroxene. We have also recalculated the glass composition from run T-4293 to be in equilibrium with an olivine of *mg*-number 90·5 (rather than the observed *mg*-number of 90), by Fe–Mg exchange, keeping the normative olivine constant. This composition is presented in Table 6 and plotted in Figs 4 and 5 as our best estimate of the solidus melt composition of MM-3 at 1·5 GPa, 1325°C.

Melting relations at 1 and 1·5 GPa for peridotite MM-3

In Figs 4 and 5 we use the calculated near-solidus melt compositions presented in Table 6 and the glass compositions from our layered reaction experiments and forward melting experiments (Table 3) to define the melting cotectics appropriate for MM-3 at 1·0 and 1·5 GPa. Although the layered reaction experiments have bulk compositions differing from MM-3, we can calculate the expected modal abundances for MM-3 at the appropriate P,T by mass balance, and these results are presented in Table 3.

Figures 4a and 5a show that the glass compositions in the Di projection define smooth melting trends at both 1·0 and 1·5 GPa starting from the nepheline-normative near-solidus liquids. The melting trend at 1·5 GPa for MM-3 matches very well the experimental data of Robinson *et al.* (1998) at 1·5 GPa for the peridotite composition T.L.

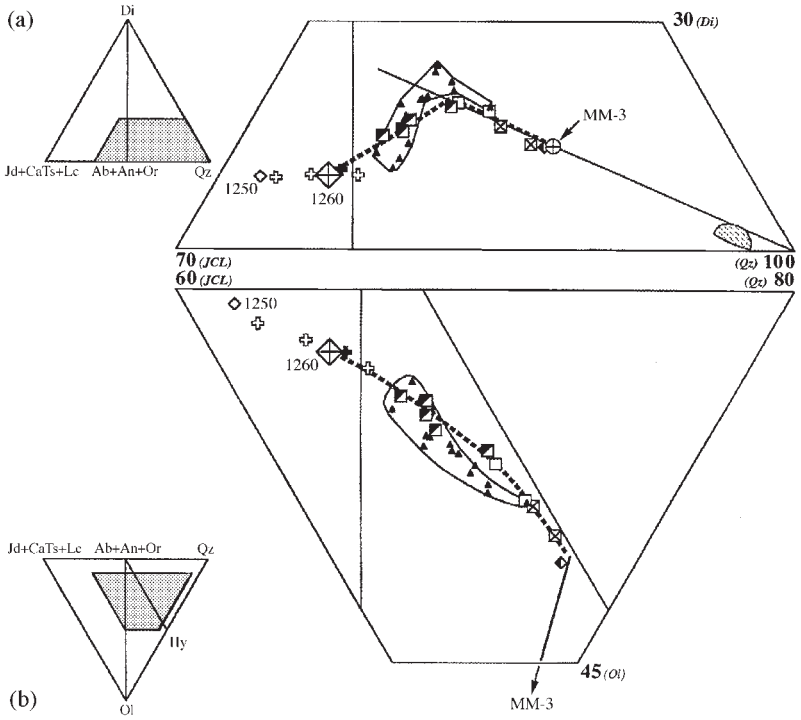

Fig. 4. Molecular normative projection from Olivine (a) onto the face [Jd + CaTs + Lc]–Di–Qz of the 'basalt tetrahedron' and from Diopside (b) onto the base [Jd + CaTs + Lc]–Qz–Ol showing glasses in peridotite melting and reaction experiments at 1·0 GPa compared with the data of Baker & Stolper (1994) and the reanalysed 70a (Baker *et al.*, 1995) glass composition of Hirschmann *et al.* (1998). Open crosses, mixed peridotite reaction experiments resulting in a plagioclase lherzolite residue [runs T-4239 and T-4248 from Falloon *et al.* (1997) and run T-4254 this study, in Table 3]; filled cross, mixed peridotite reaction experiment using the IE composition (run T-4267, Table 3); diagonally filled squares, layered peridotite reaction experiments resulting in a spinel lherzolite residue [runs T-4280, 4337, 4256, this study, Table 3, and runs T-4249 and T-4251 from Falloon *et al.* (1997)]; open squares, layered peridotite reaction experiments resulting in a spinel harzburgite residue (runs T-4281 and T-4255, Table 3); crossed squares, direct peridotite melting experiments resulting in a harzburgite residue (runs T-4243 and T-4330, Table 3); half-filled diamond, direct peridotite melting experiments resulting in a dunite residue (run T-4264, Table 3); small open diamond, the reanalysed 70a composition of Hirschmann *et al.* (1998); filled triangles, the complete data set of Baker & Stolper (1994); large crossed diamond, calculated near-solidus melt composition (Table 6); continuous line in (b) with arrow pointing to 'MM-3' is an olivine control line drawn from the Ol apex through the MM-3 bulk composition, all liquids in equilibrium with olivine only will lie on this line, for melts from peridotite MM-3; bold dashed lines in (a) and (b) are the best fit melting trends for MM-3 at 1·0 GPa; continuous line in (a) is an Hy control line drawn from the Qz apex through the peridotite composition MM-3; shaded field includes the compositions of orthopyroxene in experiments resulting in harzburgite residues at 1·0 and 1·5 GPa. For harzburgite residues in this projection the liquid composition, orthopyroxene composition and bulk composition should be collinear—as they are within the accuracy of our analytical data.

Figures 4b and 5b show the melting trend for MM-3 at 1·0 GPa and 1·5 GPa, respectively, in the Ol projection. At both 1·0 and 1·5 GPa the near-solidus melt compositions lie at relatively low normative Di contents, and as melting progresses melt compositions increase their normative diopside contents, reaching a maximum at the point of clinopyroxene elimination from the residue. After the elimination of clinopyroxene, normative diopside contents of the melts decrease along an olivine + orthopyroxene + liquid cotectic (Figs 4b and 5b), and at the point of orthopyroxene elimination the melt compositions overlie the MM-3 bulk composition in the projection from olivine. The maximum normative diopside content in the melting trends moves to higher diopside contents and closer to the Di–[Ab + An + Or]–Ol plane of critical undersaturation with increasing pressure (Fig. 5b).

Attention is drawn to the relative positions of glass compositions in equilibrium with harzburgite residues and a line from the Hy apex passing through the MM-3 composition in the olivine projection (Figs 4a and 5a). Compositions falling on this control line will have the same normative diopside to plagioclase ratio as MM-3 and this ratio is related to the CaO/Al_2O_3 ratio. However, the orthopyroxene in natural or experimental residues is not pure Hy, but contains Al_2O_3 and CaO and lower CaO/Al_2O_3 values than MM-3 (hence these pyroxenes plot below the Hy control line in Figs 4a and 5a). For harzburgite residues in this projection, the join between liquid and orthopyroxene should pass through the bulk

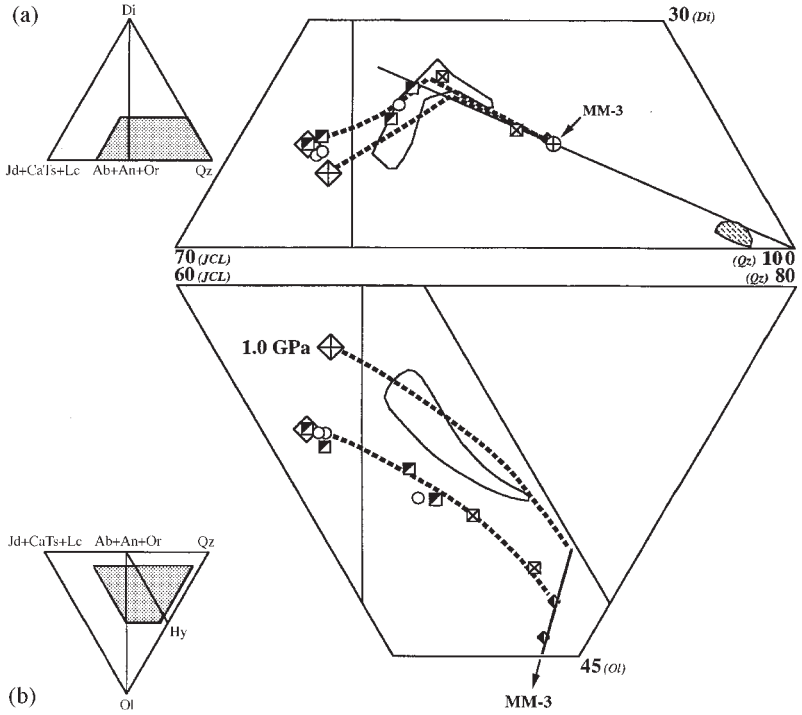

Fig. 5. Molecular normative projection from Olivine (a) onto the face [Jd + CaTs + Lc]–Di–Qz and from Diopside (b) onto the base [Jd + CaTs + Lc]–Qz–Ol of the 'basalt tetrahedron' showing glasses in peridotite melting and reaction experiments at 1·5 GPa compared with the data of Baker & Stolper (1994) (open field). Data symbols and lines are the same as for Fig. 4, plus the following: open circles, reversed glass compositions at 1·5 GPa from the peridotite composition T.L. (in Table 1) from Robinson *et al.* (1998); large open diamond, calculated near-solidus melt composition at 1·5 GPa (in Table 6).

composition, provided that spinel is absent or contains a negligible proportion of the Al_2O_3 in the composition. Glass compositions have higher CaO/Al_2O_3 ratios than MM-3 at the point of Cpx-out (~0·9 at 1 GPa; ~0·97 at 1·5 GPa) because of low CaO/Al_2O_3 ratios of residual enstatite ± spinel. However, the CaO/Al_2O_3 ratios will decrease with further melting along the olivine + orthopyroxene + liquid cotectic as the orthopyroxene in the residue becomes more refractory and the melt compositions approach the CaO/Al_2O_3 value of MM-3 (0·89).

Comparison with Baker & Stolper (1994) and Hirschmann *et al.* (1998)

In Figs 4 and 5 we compare the data of Baker & Stolper (1994) with the 1 GPa melting trend for MM-3. Figure 5 shows that the Baker & Stolper (1994) results plot between the 1·0 and 1·5 GPa melting trends for MM-3 as defined by our new experiments. It is only the highest temperature glass composition of run 26 that is convergent with the new data. The lowest temperature data (70a) of Baker *et al.* (1995) are the most divergent, entering quartz normative volume at 1250°C. However, the reanalysed 70a composition of Baker *et al.* (1995) published by Hirschmann *et al.* (1998) is in marked contrast, as it is strongly nepheline normative and plots near the melt from T-4239 (Falloon *et al.*, 1997). The new 70a composition and the original composition of Baker *et al.* (1995) both have anomalously low TiO_2 content (0·61 wt %) for a near-solidus melt (TiO_2 contents range from 1·1 to 1·7 wt % in our reaction experiments between 1250 and 1275°C) and the calculated olivine–liquid partitioning of Fe + Mg remains anomalous. For these reasons, both original and revised compositions of the melt obtained by the diamond entrapment and mineral mix starting materials remain suspect.

Experimental difficulties in previous work

In testing the published experimental data on MM-3 composition and presenting our new data as definitive, it is necessary also to attempt to understand the reasons for the incorrect results from the natural mineral mix–diamond aggregate approach. Using the normative plots of Figs 4 and 5, comparison of our data with those of Baker & Stolper (1994) shows that only the highest temperature experiment, run 26, resulted in a melt and reacted mineral compositions that approach equilibrium.

Table 7: Experimental results (KLB-1)

No.	Run no.	*T* (°C)	Run time (h)	Phase assemblage
Peridotite melting experiments				
1	T-4064	1275	92	Ol + Opx + Cpx + Sp + Plag
2	T-4066	1325	25	Ol + Opx + Cpx + L
4	T-4061	1380	24	Ol + Opx + L
5	T-4173	1500	1	Ol + L
6	T-4082	1500	1	
		1340	27	Ol + Opx + L
7	T-4129	1500	1	
		1350	24	Ol + Opx + L
8	T-4130	1500	1	
		1300	48	Ol + Opx + Cpx + Sp + L
9	KLB1-10-2	1280	336	Ol + Opx + Cpx + Sp + L
10	KLB1-10-3	1305	337	Ol + Opx + Cpx + Sp + L

Ol, olivine; Opx, orthopyroxene; Cpx, clinopyroxene; Sp, spinel; Plag, plagioclase; L, glass. Runs KLB1-10-2 and KLB1-10-3 were performed at the Department of Geological Sciences, University of Oregon at Eugene.

Even in this experiment, cores of unreacted orthopyroxene occur (Baker & Stolper, 1994). Our preferred explanation, therefore, for the anomalous data of Baker & Stolper (1994) and Baker *et al.* (1995) illustrated by the normative tetrahedron (Figs 4 and 5) is lack of equilibrium between trapped glass in the diamond aggregate and the original mineral mix. Although we do not have access to the MM-3 mineral mix, we have performed peridotite melting experiments on a very similar bulk composition, using the natural mineral mix, KLB-1 (Tables 1, 7 and 8). This natural mineral mix has been widely used for experimental work (Takahashi, 1986; Hirose & Kushiro, 1993; Takahashi *et al.*, 1993) and was prepared from a crushed spinel lherzolite xenolith from Kilbourne Hole, Arizona. The mineral assemblage of the xenolith equilibrated at ≤ 1000°C, ~1·5 GPa.

Figure 6a is a back-scattered electron image of the run product from run KLB1-10-2 (1 GPa, 1280°C, Tables 7 and 8). The run time (336 h) of KLB1-10-2 is more than an order of magnitude longer than run times used by previous workers using the KLB-1 mineral mix (Takahashi, 1986; Hirose & Kushiro, 1993) and is more than twice the run time used by Baker & Stolper (1994) at a similar temperature using the natural mineral mix MM-3 (e.g. run 55T, 1270°C, 151·3 h). Figure 6a shows that 336 h is insufficient to eliminate the presence of large unreacted clinopyroxene cores, which remain almost identical in composition to the original starting compositions (Table 8). In particular, we note the Na content of the cores, which is nearly twice that of the rims; this can create problems when Na is used to calculate melt fractions. The small melt inclusions in the clinopyroxene cores reflect the intrinsic instability of this composition (last equilibrated at ~1000°C and 1·5 GPa) at the experimental conditions of 1280°C and 1 GPa, which was described as 'early partial melting' by Doukhan *et al.* (1993). How quickly the clinopyroxene re-equilibrates depends on temperature and whether individual grains are in direct contact with melt to allow fast diffusion. In this experiment, larger clinopyroxene grains typically have an irregularly recrystallized rim <10 μm wide, but there are a few grains with a diameter of ~15 μm with little adjacent melt that have unreacted cores. Our results therefore do not support the statement of Hirose & Kushiro (1993) that 'bulk equilibrium is nearly achieved after 67 h'. In contrast to the natural mineral mix in Fig. 7a, the oxide mix derived run product MM-3 (Fig. 7b) at the same temperature shows a completely reacted assemblage uniform in the composition of all phases, with a run duration of 169 h.

The assumption used in studies utilizing natural mineral mixes is that although bulk equilibrium has clearly not been achieved, there is local equilibrium between the reacted rims of the pyroxenes and the melt phase, and the overall bulk composition has not been altered by the presence of the unreacted cores, i.e. the effective reacted composition equals the peridotite of interest. Figure 7 demonstrates that both these assumptions are unlikely to be valid. Figure 7 plots the 'reacted' rim compositions of orthopyroxene from the Baker & Stolper (1994) experiments and compares them with the orthopyroxene compositions from our synthetic peridotite

Table 8: Compositions of experimental run products (KLB-1)

Run no.	Phase	MB	Analysis	Type	SiO_2	TiO_2	Al_2O_3	Cr_2O_3	FeO	MnO	MgO	CaO	Na_2O	K_2O	P_2O_5	NiO
T-4061	Olivine	0·67(1)	EDS	A(9)	41·2(1)				8·9(2)		49·6(1)	0·28(4)				
	Orthopyroxene (KLB-1)				*54·24*	*0·11*	*4·97*	*0·34*	*6·57*	*0·16*	*32·16*	*0·85*	*0·12*			*0·11*
	Orthopyroxene (C)		EDS	A(3)	54·6(1)	0·2(1)	5·0(4)	0·7(3)	6·4(3)		32·3(2)	0·85(2)				
	Orthopyroxene (R)	0·06(2)	EDS	A(4)	56·7(5)		1·8(4)	5·3(1)		33·8(4)	1·5(1)					
	Glass	0·26(1)	WDS	A(3)	50·8(2)	0·46(1)	12·8(2)	0·45(2)	8·39(1)	0·14(3)	14·7(4)	11·2(1)	0·99(0)	0·01(1)	0·08(3)	
	Residual	**0·2321**														
T-4173	*Olivine (KLB-1)*				*39·64*		*0·03*	*0·01*	*10·52*	*0·16*	*48·25*	*0·08*	*0·01*			*0·39*
	Olivine (C)		WDS	S	40·35			0·08	9·86	0·16	49·02	0·07				0·47
	Olivine (R)		WDS	A(3)	40·99(6)			0·33(3)	7·8(2)	0·11(3)	50·2(2)	0·19(1)				0·37(6)
	Glass			n.d.												
T-4082	Olivine	0·65(1)	EDS	A(3)	40·96(6)				9·33(8)		49·6(1)	0·15(2)				
	Orthopyroxene	0·12(2)	EDS	A(2)	55·9(2)		2·5(2)	1·33(5)	5·18(1)		33·3(4)	1·84(5)				
	Glass	0·22(1)	WDS	A(5)	49·7(2)	0·55(3)	14·6(1)	0·33(7)	7·8(2)	0·17(2)	12·4(3)	13·2(1)	1·16(2)	0·01(0)	0·09(3)	
	Residual	**0·1737**														
T-4129	Olivine	0·66(2)	WDS	A(3)	40·7(3)			0·23(3)	9·3(2)	0·15(7)	49·04(9)	0·30(8)				0·33(4)
	Orthopyroxene	0·13(3)	WDS	A(2)	54·7(1)	0·09(5)	3·75(7)	1·19(5)	5·71(8)	0·16(3)	31·8(2)	2·5(1)	0·04(1)			
	Glass (DA)				*50·67*	*0·43*	*14·61*	*0·28*	*7·64*	*0·13*	*13·39*	*11·17*	*1·5*	*0·19*		
	Glass	0·21(2)	WDS	A(7)	50·0(2)	0·53(3)	14·3(4)	0·32(4)	7·9(2)	0·14(4)	12·9(6)	12·6(3)	1·19(2)	0·03(1)	0·07(4)	
	Residual	**0·2684**														
T-4130	Olivine		WDS	A(3)	40·6(1)			0·09(2)	10·0(1)	0·17(3)	48·6(1)	0·29(2)				0·29(5)
	Orthopyroxene		WDS	Sel	53·08	0·15	6·88	0·95	5·78	0·14	30·35	2·6	0·07			
	Clinopyroxene		WDS	Sel	50·5	0·25	7·85	0·99	4·28	0·15	19·36	16·28	0·33			
	Spinel		WDS	S	0·16	0·08	58·71	10·76	8·55		21·72	0·03				
	Glass (DA)				*50·49*	*0·65*	*17·94*	*0·11*	*6·69*	*0·11*	*10·08*	*11·37*	*2·47*	*0·09*		
	Glass	n.d.														
KLB1-10-2	*Olivine (KLB-1)*				*39·64*		*0·03*	*0·01*	*10·52*	*0·16*	*48·25*	*0·08*	*0·01*			*0·39*
	Olivine		WDS	A(2)	40·1(3)			0·05(1)	10·1(2)	0·13(1)	49·01(3)	0·17(5)				0·37(4)
	Orthopyroxene (KLB-1)				*54·24*	*0·11*	*4·97*	*0·34*	*6·57*	*0·16*	*32·16*	*0·85*	*0·12*			*0·11*
	Orthopyroxene (C)		WDS	A(2)	53·8(5)	0·06(2)	5·1(1)	0·37(3)	6·9(3)	0·14(6)	32·6(1)	0·84(1)	0·10(4)			
	Orthopyroxene (R)		WDS	A(3)	53·8(3)	0·10(5)	5·1(2)	0·43(5)	6·8(3)	0·16(4)	32·6(1)	0·96(2)	0·08(2)			
	Clinopyroxene (KLB-1)				*51·3*	*0·58*	*7·4*	*0·78*	*3·11*	*0·1*	*14·7*	*19·54*	*1·72*			*0·11*
	Clinopyroxene (C)		WDS	Sel	51·9	0·63	7·1	0·69	3·68	0·13	15·85	19·57	1·16			
	Clinopyroxene (R)		WDS	A(3)	51·1(3)	0·32(2)	6·8(2)	0·92(6)	4·1(2)	0·12(3)	18·8(1)	17·2(2)	0·63(5)			
	Spinel (KLB-1)				*0·06*	*0·11*	*58·48*	*7·82*	*10·68*		*21·61*					*0·43*
	Spinel (C)		WDS	S	0·06	0·16	60·21	8·89	8·56	0·1	22·02					
	Spinel (R)		WDS	A(4)	0·15(1)	0·11(4)	56·3(5)	12·7(3)	9·3(1)	0·05(4)	21·39(7)					
	Glass			n.d.												

Run no.	Phase	MB	Analysis	Type	SiO_2	TiO_2	Al_2O_3	Cr_2O_3	FeO	MnO	MgO	CaO	Na_2O	K_2O	P_2O_5	NiO
KLB1-10-3	*Olivine (KLB-1)*				*39·64*		*0·03*	*0·01*	*10·52*	*0·16*	*48·25*	*0·08*	*0·01*			*0·39*
	Olivine		WDS	A(8)	40·1(2)			0·08(2)	10·2(1)	0·15(3)	48·9(2)	0·24(4)				0·34(2)
	Orthopyroxene (KLB-1)				*54·24*	*0·11*	*4·97*	*0·34*	*6·57*	*0·16*	*32·16*	*0·85*	*0·12*			*0·11*
	Orthopyroxene (C)		WDS	A(4)	53·9(2)	0·12(2)	5·1(1)	0·36(3)	6·8(1)	0·13(2)	32·62(8)	0·84(4)	0·11(1)			
	Orthopyroxene (R)		WDS	A(6)	53·4(3)	0·16(3)	5·4(6)	0·6(2)	6·5(3)	0·13(3)	31(1)	2·2(9)	0·13(5)			
	Clinopyroxene (KLB-1)				*51·13*	*0·58*	*7·4*	*0·78*	*3·11*	*0·1*	*14·7*	*19·54*	*1·72*			*0·11*
	Clinopyroxene (C)		WDS	A(2)	51·5(3)	0·55(1)	7·2(4)	0·73(4)	3·43(3)	0·09(0)	16·1(9)	19·42(5)	1·0(2)			
	Clinopyroxene (R)		WDS	A(7)	51·3(6)	0·3(1)	6·4(9)	1·0(1)	4·3(4)	0·13(5)	19·1(1)	17(1)	0·5(2)			
	Spinel (KLB-1)				*0·06*	*0·11*	*58·48*	*7·82*	*10·68*		*21·61*					*0·43*
	Spinel		WDS	A(3)	0·13(2)	0·16(3)	54(2)	16(2)	9·6(4)	0·02(2)	20·8(4)					
	Glass			n.d.												

Numbers in parentheses next to each analysis or mass balance are 1σ in terms of the last units cited. Mass balance in weight fraction was performed using least-squares linear regression using the software PETMIX and 'Residual' refers to the square of the sum of the residuals. MB, mass balance using the KLB-1 bulk composition. WDS, wavelength-dispersive microanalysis using Cameca SX-50 microprobes housed in either the Central Science Laboratory, University of Tasmania (operating conditions 15 kV, 20 ηA) or the Department of Geological Sciences, University of Oregon at Eugene (operating conditions 15 kV, 20 ηA). EDS, energy-dispersive microanalysis using a Cameca MICROBEAM microprobe housed in the Research School of Earth Sciences, The Australian National University (operating conditions 15 kV, 5 ηA). All glass analyses have been normalized to the composition of international glass standard VG-2 (Jarosewich *et al.*, 1980), which was analysed together with the glasses under the same analytical conditions. 'Type' refers to whether the analysis given is an average (A) with the number used to form the average given in parentheses; Sel refers to a selected analysis. The selected pyroxene core analyses demonstrate the most unreacted compositions obtained; n.d., not determined; S, only a single analysis was obtained. Data in italic type with label '(KLB-1)' are the composition of the starting minerals in the KLB-1 mineral mix (Hirose & Kushiro, 1993). Glass data in italic type with label '(DA)' are the compositions of the glass trapped in the diamond aggregate experiments of Hirose & Kushiro (1993) at the same temperature as our experiments (Table 7).

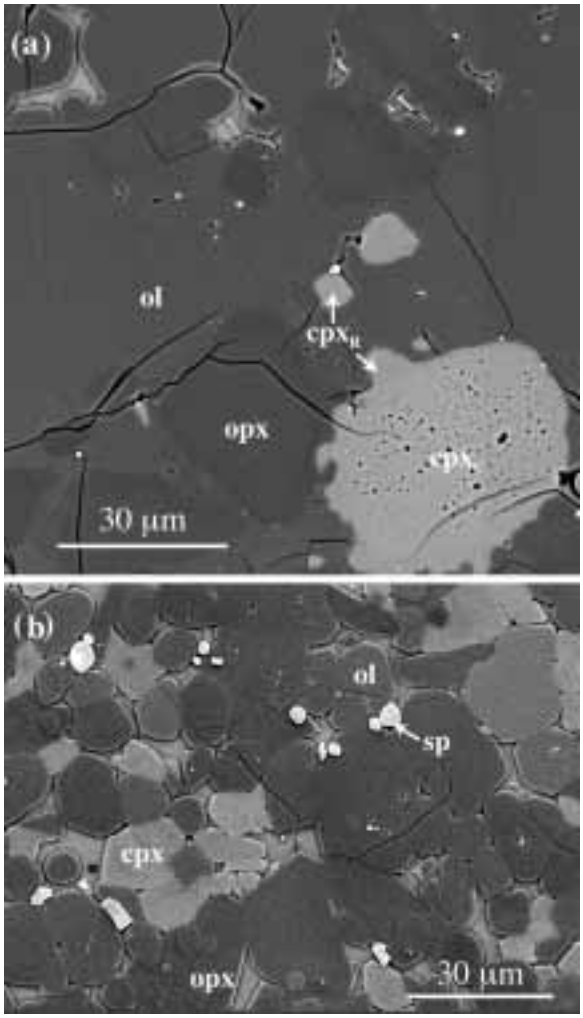

Fig. 6. Back-scattered electron images comparing the differences in run products resulting from the use of natural mineral mix (KLB-1, a) vs synthetic mix (MM-3, b) starting materials at the same pressure and temperature (1·0 GPa, 1280°C). Run KLB1-10-2 (a, Tables 7 and 8) clearly shows that clinopyroxene grains (light grey) and orthopyroxene (darker grey) have not equilibrated to ~20 μm. It should be noted in particular that clinopyroxene grain interiors (bottom right) have unequilibrated pockets of 'internal' melt as described by Doukhan *et al.* (1993). In contrast, run MM3-3 (b, Tables 2 and 3) shows a well-equilibrated run product; light grey, clinopyroxene; darker grey, olivine and orthopyroxenes (orthopyroxene poikilitic to olivine, bottom centre); bright, spinel.

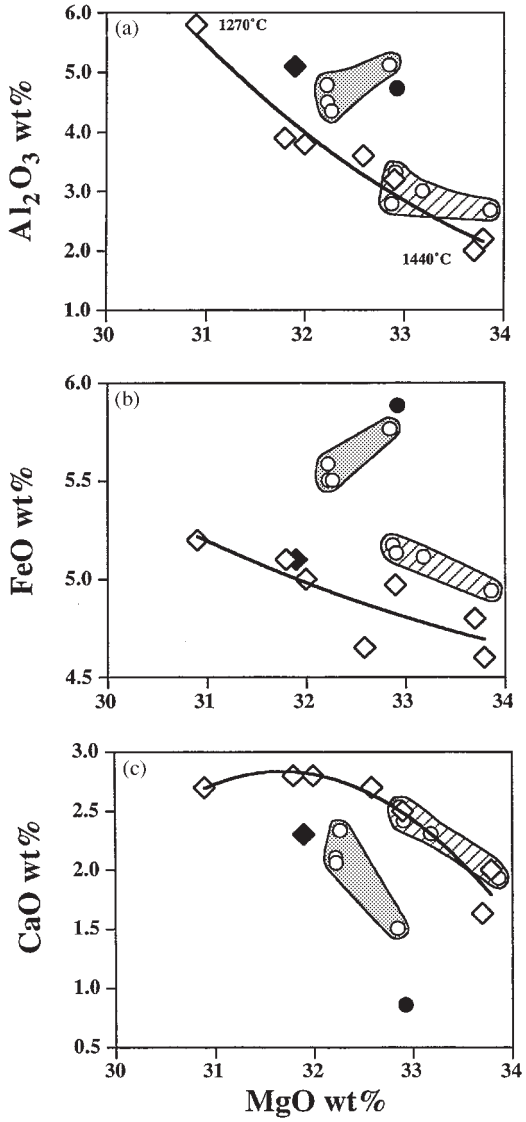

Fig. 7. Al_2O_3 (a), FeO (b) and CaO (c) contents (wt %) vs MgO (wt %) of above-solidus orthopyroxenes in our peridotite melting experiments (open diamonds) compared with the data (open circles) of Baker & Stolper (1994). It should be noted that the orthopyroxene compositions of Baker & Stolper (1994) fall into two distinct groups (<1300°C, shaded fill; >1300°C, diagonal fill) and that the orthopyroxene compositions at temperatures <1300°C plot close to the orthopyroxene composition in the MM-3 mineral mix (filled circle). Bold line shows the best fit trend for orthopyroxene compositions with temperature in our above-solidus experiments and the filled diamond is the subsolidus orthopyroxene from run T-4193 (Tables 2, 3 and 9).

melting experiments at 1 GPa. The data from Baker & Stolper (1994) can be divided into two groups. Data for <1300°C plot close to the initial orthopyroxene of the mineral mix, whereas data for >1300°C plot close or parallel to our data. This suggests that it is only at temperatures >1300°C that the 'reacted' part of the mineral mix approaches equilibrium compositions. However, this will not necessarily mean that the glass compositions will be appropriate for 1 GPa melting of MM-3 at >1300°C, because of two effects. The first is obvious, as the presence of unreacted starting materials will change the effective bulk composition relative to MM-3. The second is illustrated in Table 9, which compares the mineral compositions and modal proportions of the subsolidus, equilibrated MM-3 composition at 1·0 and 1·5 GPa with those of the mineral mix MM-3. The mineral mix more closely resembles the

Table 9: Compositions from subsolidus runs at 1250°C at 1·0 and 1·5 GPa and the MM-3 natural mineral mix

	Olivine			Opx			Cpx			Spinel			Plagioclase
	1·0 GPa A(7)	1·5 GPa A(5)	MM-3 A(4)	1·0 GPa A(3)	1·5GPa A(6)	MM-3 A(8)	1·0 GPa A(4)	1·5 GPa A(9)	MM-3 A(9)	1·0 GPA A(3)	1·5 GPa A(3)	MM-3 A(5)	1·0 GPa A(7)
SiO_2	40·8(1)	40·9(1)	40·4(1)	53·9(8)	53·0(5)	54·7(2)	51·4(2)	51·4(4)	51·8(1)		0·8(2)	0·04(1)	54·9(6)
TiO_2				0·25(5)	0·26(3)	0·11(1)	0·54(5)	0·48(8)	0·43(8)	0·29(3)	0·28(0)	0·12(1)	
Al_2O_3				5·1(6)	6·1(4)	4·73(7)	5·9(3)	6·9(5)	6·8(1)	51·5(9)	54·6(2)	54·99(3)	28·3(4)
Cr_2O_3	0·13(4)	0·12(2)	0·03(1)	0·87(5)	0·78(8)	0·49(1)	1·13(8)	1·1(1)	1·09(2)	17·1(8)	13·41(1)	13·00(8)	
FeO	9·2(1)	9·1(1)	9·20(9)	5·4(4)	5·7(2)	5·88(4)	3·4(2)	3·7(3)	2·85(11)	8·9(1)	8·75(4)	10·39(6)	0·47(3)
MnO	0·17(3)	0·13(2)	0·14(1)	0·15(3)	0·13(3)	0·14(1)	0·12(4)	0·14(3)	0·08(2)		0·16(1)	0·10(1)	
MgO	49·5(1)	49·55(6)	49·80(8)	31·9(7)	32·1(8)	32·9(2)	19·1(4)	19·0(7)	15·7(1)	22·1(4)	21·9(1)	21·01(3)	0·3(1)
CaO	0·23(2)	0·24(2)	0·08(1)	2·3(2)	1·8(2)	0·86(2)	17·8(7)	16·4(9)	19·6(2)	0·13(2)	0·15(7)		11·2(5)
Na_2O				0·08(1)	0·15(1)	0·12(1)	0·61(3)	0·93(5)	1·62(6)				4·8(3)
mg-no.	90·55	90·65	90·6	91·32	90·94	90·88	90·92	90·15	90·75	81·57	81·68	78·3	An 56·3
Mode	55(1)	50·6(4)	50	26(2)	29·5(8)	30	13·4(7)	17·8(5)	17	1·4(3)	1·7(1)	3	4·2(9)

MM-3 natural mineral mix data from Baker & Stolper (1994). Other details as for Tables 1 and 3.

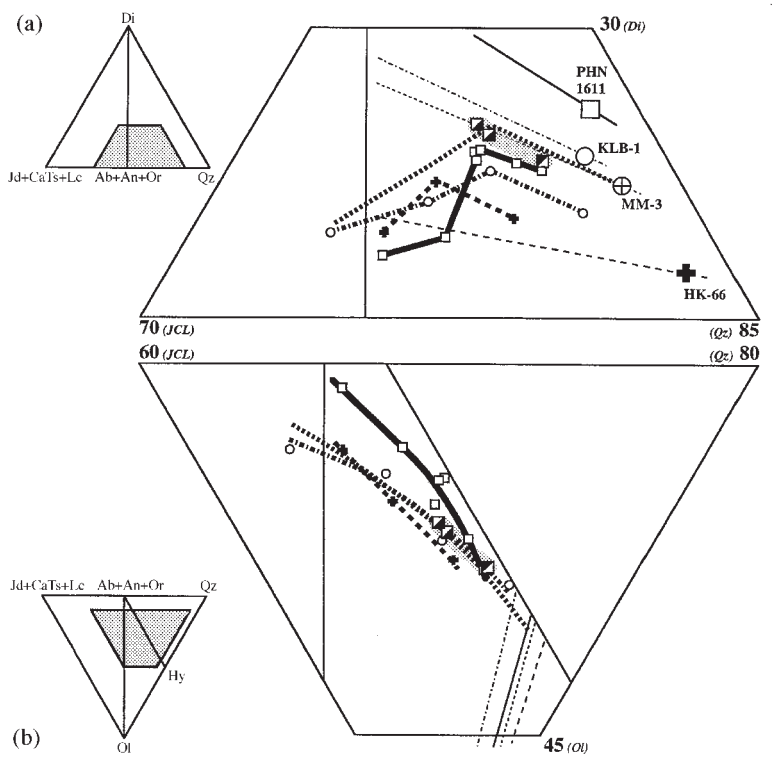

Fig. 8. Molecular normative projection from Olivine (a) onto the face [Jd + CaTs + Lc]–Di–Qz and from Diopside (b) onto the base [Jd + CaTs + Lc]–Qz–Ol of the 'basalt tetrahedron' comparing experimental glass compositions produced by the natural mineral mix–diamond aggregate technique at 1·0 GPa with the melting trend of MM-3 at 1·0 GPa. Open squares, glass compositions from peridotite PHN1611 (Kushiro, 1996), larger symbol in (a) is the peridotite PHN1611, fine continuous line is an Hy control line in (a) and an olivine control line in (b); open circles, glass compositions from peridotite KLB-1 (Hirose & Kushiro, 1993), larger symbol in (a) is the peridotite KLB-1, fine dash–dot–dash line is an Hy control line in (a) and an olivine control line in (b); open circle with cross, peridotite MM-3, bold dashed line is the melting trend for MM-3 at 1·0 GPa (this study), fine short-dashed line is an Hy control line in (a) and an olivine control line in (b); filled crosses, glass compositions from peridotite HK66 (Hirose & Kushiro, 1993), larger symbol in (a) is the peridotite HK66, fine long-dashed line is an Hy control line in (a) and an olivine control line in (b); bottom filled squares, KLB-1 reversal experiments (runs T-4082 and T-4129, Tables 7 and 8); top filled square, run T-4061 (Tables 7 and 8).

1·5 GPa than the 1·0 GPa assemblage, except for Na and Ca contents in clinopyroxene, and Ca and Al contents in orthopyroxene. Plagioclase is absent in the mineral mix but should be present at the solidus at 1 GPa. The diamond aggregate appears to entrap and preserve an initial melt, from an inappropriate modal mineralogy, from further reaction and equilibration.

As a result of these uncertainties we recommend that results obtained from peridotite melting studies at 1 GPa utilizing natural mineral mixes as starting material should be treated with caution. The uncertainties inherent in the use of crushed mineral mixes of grain size ≥ 10 μm, of time-dependent pressure changes in the diamond aggregate and of time-dependent reactions of minerals and melts, together mean that melt compositions must be confirmed by reversals or the melt–source sandwich approach.

Comparison with other diamond-aggregate studies at 1 GPa

In this study we have tested the data of Baker & Stolper (1994) because that was the most fully documented study published to date. However, there have been two other published studies using the same natural mineral mix–diamond aggregate entrapment technique (Hirose & Kushiro, 1993; Kushiro, 1996), and it is important to know whether the same problems of disequilibrium clearly evident in the data of Baker & Stolper (1994) and Baker *et al.* (1995) are present in these data sets as well. In Fig. 8 we compare the 1 GPa partial melt compositions from three peridotite compositions (KLB-1, HK-66 and PHN1611) with the MM-3 1 GPa melting trend. In the projection from Di (Fig. 8b) the melting trends for KLB-1 and HK-66 appear to be generally consistent with the melting trend for MM-3 at 1 GPa, and differences in

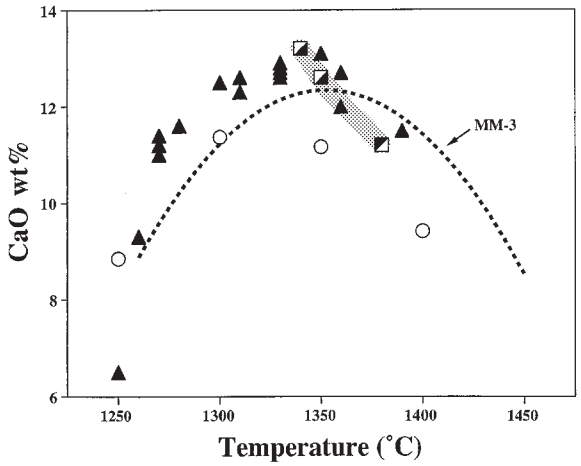

Fig. 9. CaO wt % vs temperature (°C) showing the comparison between the glass compositions of Hirose & Kushiro (1993) from KLB-1 at 1·0 GPa (open circles) and our reversal and direct melting experiments on KLB-1 (half-filled squares). Filled triangles are the data of Baker & Stolper (1994) and the reanalysed 1250 and 1260°C compositions from Hirschmann *et al.* (1998), from MM-3 mineral mix. Dashed line is the locus of glass compositions determined for MM-3 composition in this study (Table 3).

orientation could be simply due to differences in bulk composition. For example, PHN1611 partial melt compositions have higher K_2O contents (Kushiro, 1996) and this may be the cause for the significantly different position of the PHN1611 melting trend in the Di projection (Fig. 8b). This projection illustrates the position of olivine–pyroxene cotectic but does not illustrate relative proportions of pyroxene components nor the important CaO/Al_2O_3 ratio of sources and liquids. These factors are illustrated by Fig. 8a.

In this projection, peridotite PHN1611 has the highest normative Di content, and the highest CaO/Al_2O_3 value, yet high-degree melts of this composition, reportedly in equilibrium with harzburgite, all have lower normative Di contents than melts from MM-3 (Fig. 8a). A similar behaviour is also evident for the experimental data from peridotite KLB-1 (Fig. 8a). For both compositions, the absence of collinearity in liquid, bulk and orthopyroxene compositions in Fig. 8a is evidence for error in either the reacting composition or determination of melt compositions. Melt compositions from HK-66 show a different behaviour in that high-degree melts in equilibrium with harzburgite have high CaO/Al_2O_3 values, lying on the diopside-rich side of an Hy-control line appropriate for HK-66 but approximating collinearity for liquid, bulk and orthopyroxene compositions. For melt compositions from PHN1611 and KLB-1 it is impossible to obtain mass balance if the high-temperature partial melt compositions have harzburgite residues, as reported (Hirose & Kushiro, 1993; Kushiro, 1996). These inconsistencies have been previously noted by Baker & Stolper (1994) in terms of the unexpectedly low CaO contents of KLB-1 glass compositions compared with MM-3, as both compositions have similar CaO/Al_2O_3 values (Figs 8 and 9).

In Fig. 9, we plot the CaO data of Baker & Stolper (1994) vs reported temperature and compare with data from KLB-1 (Hirose & Kushiro, 1993). Both data sets show maxima in CaO content vs temperature but the KLB-1 liquids define a trend that is anomalously low in CaO. In Figs 8 and 9, we also plot the results of one direct melting experiment on the KLB-1 mineral mix at 1380°C (run T-4061, Tables 7 and 8) and two reversal experiments on the KLB-1 mineral mix at temperatures of 1340–1350°C (runs T-4082 and T-4129, Tables 7 and 8). The direct melting experiment on KLB-1 at 1380°C resulted in a high degree of melting (~26 wt %, Table 8) and a harzburgite residue. The residual orthopyroxene still retained unreacted cores (Table 8). In the reversal experiments, the KLB-1 mineral mix was first held at a temperature of 1500°C, for 1 h, before the temperature was lowered to the desired run temperature. Holding the KLB-1 mineral mix at 1500°C for 1 h results in an olivine + liquid assemblage in which all except cores of coarse olivine has reacted (see run T-4173, Tables 7 and 8). However, because all pyroxenes have been eliminated from the residue, orthopyroxene crystallizes from the melt phase when temperature is lowered. This results in orthopyroxenes that are free of relict cores from the mineral mix. In Fig. 8a, the glasses from these three experiments on KLB-1 mineral mix define an olivine + orthopyroxene + liquid cotectic plotting at significantly higher normative Di than the Hirose & Kushiro (1993) glasses but still below the MM-3 melting trend and an Hy control line through KLB-1. In Fig. 9 the glasses from our experiments plot at significantly higher CaO contents and overlie the MM-3 data from Baker & Stolper (1994). Our results demonstrate that the glass compositions of Hirose & Kushiro (1993) are not equilibrium melts of peridotite KLB-1. In addition, our reversals strongly suggest that our particular batch of mineral mix KLB-1 has a composition different from that published by Takahashi (1986), as our reversals define a melting trend falling below an Hy control line through the nominal composition of KLB-1 (Fig. 8a). It is also interesting to compare the glass in the direct melting experiment T-4061 with the high-degree melting experiments of Hirose & Kushiro (1993). Run T-4061 was run for a length of time similar to that of the Hirose & Kushiro (1993) experiments at these temperatures (24 h) and has unreacted orthopyroxene cores, although Hirose & Kushiro (1993) reported minimal zoning of minerals. The glass in T-4061 was analysed from melt pools in direct contact with olivine and the rims of reacted orthopyroxenes, whereas the glass in the Hirose & Kushiro (1993) experiments is that present in the diamond aggregate after the experiment. The differences

Table 10: Comparison of calculated model melts and experimental melts at 1·0 GPa

Residue:	T-4254 Pl lherzolite	K&G (1992) Pl lherzolite	T-4256 Sp lherzolite	K&G (1992) Sp lherzolite	K (1997) Sp lherzolite	MELTS Sp lherzolite	N (1997) Sp Lherzolite
SiO_2	50·86	51·52	50·20	49·75	48·68	49·33	51·30
TiO_2	1·37	1·34	0·59	0·58	0·58	0·81	0·51
Al_2O_3	18·57	17·56	14·60	16·70	11·72	18·05	14·13
FeO	7·39	7·69	6·90	6·52	8·45	5·07	6·48
MgO	7·87	8·19	13·20	12·48	16·17	10·29	12·39
CaO	9·62	9·64	12·80	12·84	12·81	10·21	13·08
Na_2O	4·04	4·05	1·12	1·12	1·10	6·04	1·38
mg-no.	65·49	65·49	77·32	77·32	77·32	78·34	77·31
T (°C)	1270	1255	1350	1294	1325	1350	1350

K&G (1992), model of Kinzler & Grove (1992); K (1997), model of Kinzler (1997); N (1997), model of Niu (1997) [which is an improved version of Niu & Batiza (1991); Y. Niu, (personal communication, 1998)]; MELTS, model of Ghiorso & Sack (1995). The composition N (1997) was calculated by adjusting the percent melting [input for the Niu (1997) calculation], until the calculated model temperature of Niu (1997) equalled 1350°C (21% melting). Runs T-4254 and T-4256 (Tables 1 and 3) were used as input to calculate the model melts of Kinzler & Grove (1992) [equations (2)–(5) for Pl lherzolite and equations (7)–(10) for Sp lherzolite, Kinzler & Grove (1992)] and Kinzler (1997) [table 5, Kinzler (1997) and R. J. Kinzler (personal communication, 1998)]. It should be noted that the temperatures listed for K&G (1992) and K (1997) are model calculated temperatures using the composition of runs T-4254 and T-4256 as input. MELTS (Ghiorso & Sack, 1995) composition was calculated using an IW (iron–wüstite) fO_2 path.

Table 11: Comparison of calculated model melts and experimental melts at 1·5 GPa, 1325 (°C)

	T-4293	Run 64	K&G (1992)	K (1997)	N (1997)
SiO_2	49·10	49·00	49·05	47·64	49·40
TiO_2	1·08	1·19	1·06	1·05	0·87
Al_2O_3	18·10	18·40	19·15	17·36	17·83
FeO	6·90	6·47	6·60	7·93	6·35
MgO	10·60	11·10	10·13	12·19	10·13
CaO	10·30	10·20	10·23	10·13	10·84
Na_2O	3·80	3·66	3·78	3·70	3·04
mg-no.	73·24	75·35	73·23	73·26	73·97
T (°C)	1325	1325	1338	1356	1325

K&G (1992), model of Kinzler & Grove (1992); K (1997), model of Kinzler (1997); N (1997), model of Niu (1997) [which is an improved version of Niu & Batiza (1991); Y. Niu (personal communication, 1998)]. The composition N (1997) was calculated by adjusting the percent melting [input for the Niu (1997) calculation], until the calculated model temperature of Niu (1997) equalled 1325°C (7% melting). Run T-4293 (Tables 1 and 3) was used as input to calculate the model melts of Kinzler & Grove (1992) [equations (7)–(10), Kinzler & Grove (1992)] and Kinzler (1997) [table 5, Kinzler (1997) and R. J. Kinzler (personal communication, 1998)]. It should be noted that the temperatures listed for K&G (1992) and K (1997) are model calculated temperatures using the composition of run T-4293 as input. Run 64 is from Robinson *et al.* (1998) and is a liquid in equilibrium with a spinel lherzolite residue at 1·5 GPa, 1325°C from melting experiments on peridotite T.L. (Table 1), shown for comparison.

in composition suggest that the entrapped melt in the diamond aggregate preserves a disequilibrium melt, segregated early in the experiment and not re-equilibrated to the changes in residual mineralogy.

In summary, it is clear from Fig. 8 and our experiments on the KLB-1 mineral mix at 1·0 GPa that the natural mineral mix–diamond aggregate entrapment technique as used in the studies of Hirose & Kushiro (1993) and

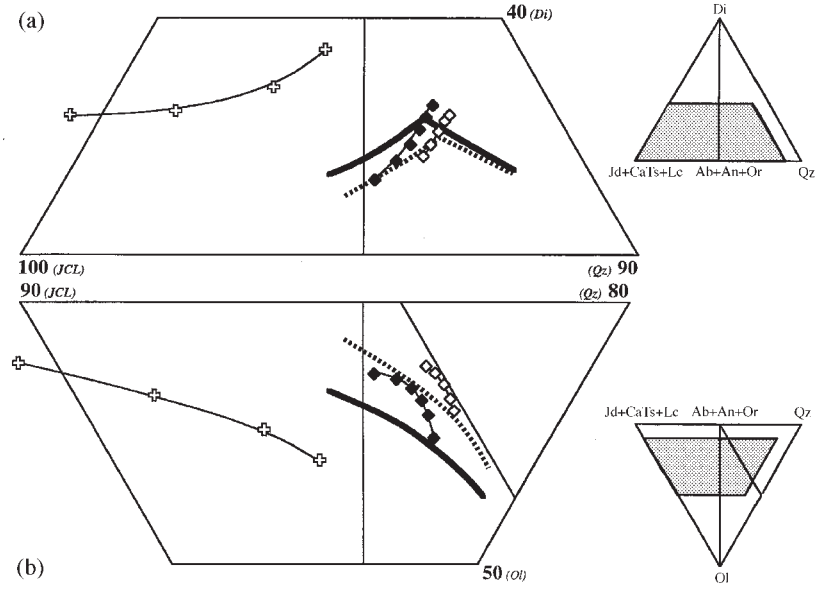

Fig. 10. Molecular normative projection from Olivine (a) onto the face [Jd + CaTs + Lc]–Di–Qz and from Diopside (b) onto the base [Jd + CaTs + Lc]–Qz–Ol of the 'basalt tetrahedron' comparing model melt compositions of MM-3 with the experimentally determined melting trends at 1·0 and 1·5 GPa. Open diamonds, 1·0 GPa melts (model temperatures 1308–1400°C) calculated using Niu (1997); filled diamonds, 1·5 GPa melts (model temperatures 1325–1450°C) calculated using Niu (1997); open crosses, 1·0 GPa melts (model temperatures 1325–1400°C) calculated using MELTS (Ghiorso & Sack, 1995); bold dashed line and bold continuous lines are the melting trends for MM-3 at 1·0 GPa and 1·5 GPa, respectively (this study)

Kushiro (1996) has failed to produce equilibrium partial melts of the respective peridotite compositions chosen for study (HK-66, KLB-1; PHN1611). It is therefore recommended that these data sets should be used with caution. It is also clear that the use of natural mineral mixes and diamond aggregate entrapment technique is not an appropriate method for determining the compositions of high-pressure mantle melts. Studies using this approach must be confirmed by the reversal and source–melt sandwich experiments described in this paper. The diamond aggregate techniques for melt entrapment must be further tested to isolate the effects of mineral mix vs sintered oxide starting mixes, the elimination of a pressure gradient within the aggregate before melting and variations of melt compositions within the aggregate vs melt compositions in the surrounding peridotite.

Status of parameterized mantle melting models

A number of workers have drawn on published experimental data to present numerical melting models that can calculate partial melt compositions given a specific peridotite bulk composition (Kinzler & Grove, 1992; Ghiorso & Sack, 1995; Kinzler, 1997; Niu, 1997). These melting models are used to calculate the composition of aggregated melt compositions resulting from dynamic melting of upwelling mantle peridotite. In Figs 10–12, and Tables 10 and 11, we show a comparison between the different numerical models and their ability to match our experimental data on MM-3 at 1·0 and 1·5 GPa.

In Fig. 10 we compare the melting trends for MM-3 at 1·0 and 1·5 GPa with the calculated melting trends for MM-3 using the models of Ghiorso & Sack (1995) and Niu (1997). The comparison shows that the MELTS program (Ghiorso & Sack, 1995) at 1·0 GPa predicts a matching shape to the lherzolite melting trend of MM-3 within the basalt tetrahedron but the calculated compositions are excessively olivine rich, silica undersaturated and much too high in normative diopside (Fig. 10, Table 10). The numerical model of Niu (1997) converges on the experimental data at higher temperature in the projection from diopside (Fig. 10b) and matches the shape of the melting trends in the projection from olivine (Fig. 10a) in terms of increasing normative diopside as melting progresses towards cpx-out. However, the trends are displaced away from the [Jd + CaTs + Lc] apex towards the [Qz] apex.

Both Kinzler & Grove (1992) and Kinzler (1997) provided numerical models that calculate the compositions of melt in equilibrium with a spinel or plagioclase lherzolite residue, and Figs 11 and 12 show a direct comparison between our experimental glass compositions and those calculated by these numerical models. The

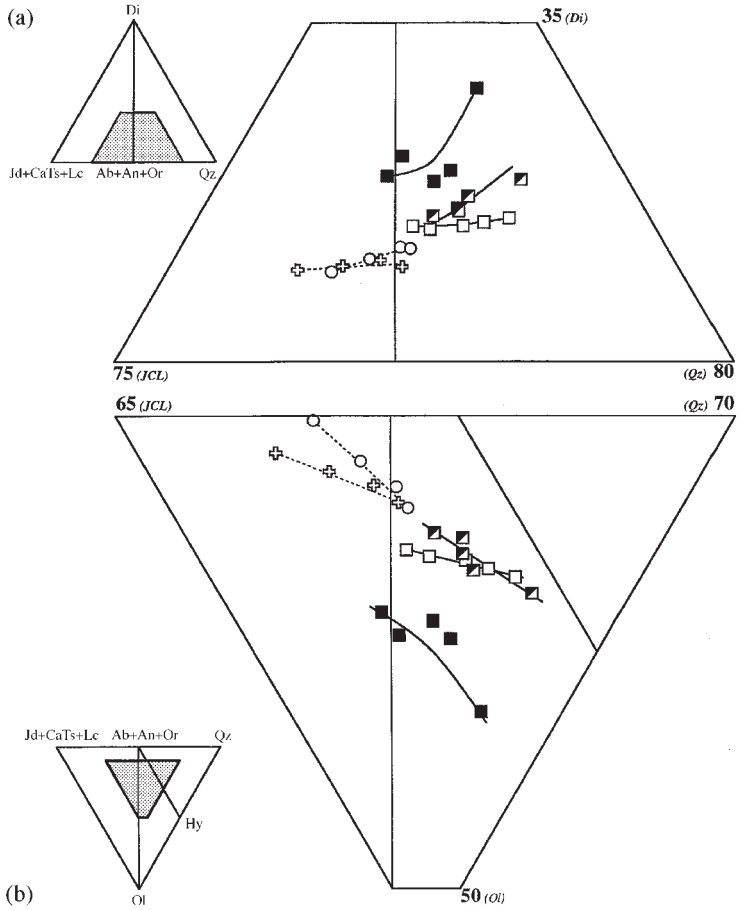

Fig. 11. Molecular normative projection from Olivine (a) onto the face [Jd + CaTs + Lc]–Di–Qz and from Diopside (b) onto the base [Jd + CaTs + Lc]–Qz–Ol of the 'basalt tetrahedron' comparing model melt compositions of MM-3 with the experimentally determined melting trends at 1·0 GPa. Open crosses, mixed peridotite reaction experiments at 1·0 GPa resulting in a plagioclase lherzolite residue [this study and Falloon *et al.* (1997)]; open circles, model plagioclase lherzolite liquids at 1·0 GPa calculated using equations (2)–(5) of Kinzler & Grove (1992); diagonally filled squares, layered peridotite reaction experiments at 1·0 GPa resulting in a spinel lherzolite residue [this study and Falloon *et al.* (1997)]; open squares, model spinel lherzolite liquids at 1·0 GPa calculated using equations (7)–(10) of Kinzler & Grove (1992); filled squares, model spinel lherzolite liquids at 1·0 GPa calculated using equations in table 5 of Kinzler (1997) (and R. J. Kinzler, personal communication, 1998).

calculated liquids (Kinzler & Grove, 1992) in equilibrium with plagioclase lherzolite at 1·0 GPa provide a reasonable approximation to our liquids in both the Di and Ol projections (Fig. 11). However, the calculated liquids in equilibrium with spinel lherzolite at 1·0 and 1·5 GPa do not (Figs 11 and 12, Tables 10 and 11). The Kinzler & Grove (1992) model calculates liquids that in the projection from Diopside are too rich in normative olivine at 1·0 GPa (Fig. 11b) and too olivine poor at 1·5 GPa (Fig. 12b), and in the projection from Olivine both the 1·0 GPa (Fig. 11a) and 1·5 GPa (Fig. 12a) trends do not show the increasing normative diopside towards the point of cpx-out. The calculated 1·5 GPa liquids incorrectly plot at lower normative diopside contents than the calculated 1·0 GPa liquids (Fig. 12a). Also shown in Figs 11 and 12 are the calculated model liquids of Kinzler (1997) at 1·0 and 1·5 GPa. The calculated model liquids are too olivine normative with respect to the experimental liquids in the projection from Diopside (Figs 11b and 12b), and in the Olivine projection, although they show increasing normative diopside, the calculated liquids have excessively high diopside values (Figs 11a and 12a).

In summary, none of the above melting models produces a close matching to our experimental data. In general, the Niu (1997) melting model gives the closest result to our experimental data (Fig. 10, Tables 10 and 11).

CONCLUSIONS

(1) In a study of lherzolite (MM-3 composition) melting behaviour at 1·0 and 1·5 GPa, under anhydrous conditions, we have defined the range of melt compositions from the solidus to the production of dunitic residue. In

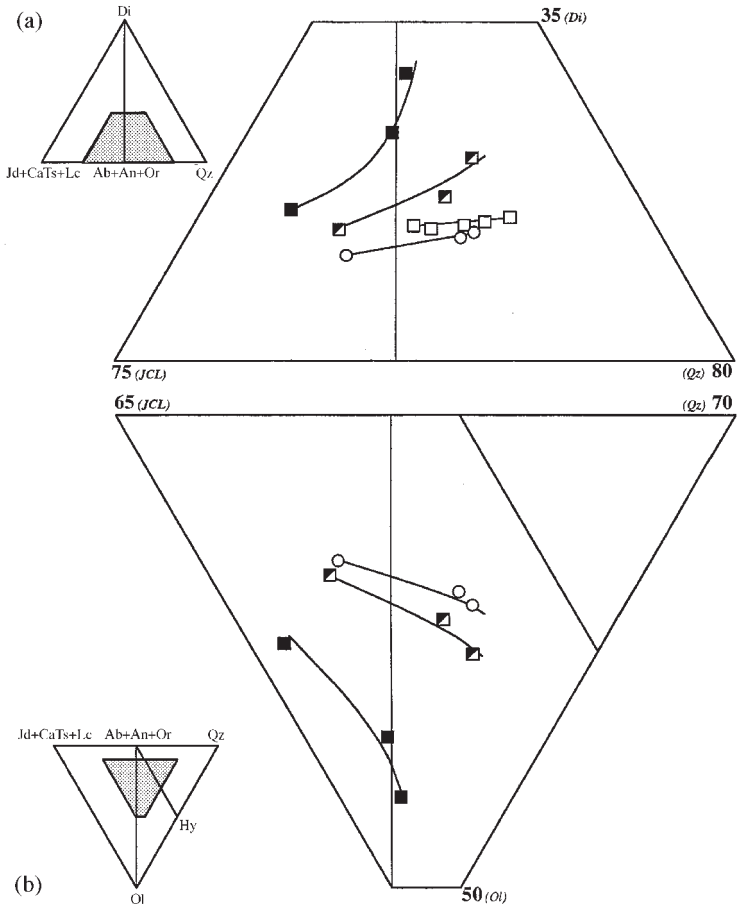

Fig. 12. Molecular normative projection from Olivine (a) onto the face [Jd + CaTs + Lc]–Di–Qz and from Diopside (b) onto the base [Jd + CaTs + Lc]–Qz–Ol of the 'basalt tetrahedron' comparing model melt compositions of MM-3 with the experimentally determined melting trends at 1·5 GPa. Diagonally filled squares, mixed and layered reaction experiments at 1·5 GPa resulting in a lherzolite ± spinel residue; open circles, model spinel lherzolite liquids at 1·5 GPa calculated using equations (7)–(10) of Kinzler & Grove (1992); filled squares, model spinel lherzolite liquids at 1·5 GPa calculated using equations in table 5 of Kinzler (1997) (and R. J. Kinzler, personal communication). Also shown in (a) are the model spinel lherzolite liquids (open squares) at 1·0 GPa calculated using equations (7)–(10) of Kinzler & Grove (1992) (from Fig. 11a).

conducting our investigation we found it necessary to evaluate and eventually discard all but the highest temperature experiment of a previous experimental study of melting of MM-3 using crushed natural minerals and a diamond aggregate melt entrapment approach. Our results demonstrate that mineral mixes are not a suitable starting material for peridotite melting studies at 1·0 GPa, that studies utilizing natural mineral mixes should be treated with caution, and that in general natural mineral mixes are not suitable materials for experimental studies. The use of diamond aggregate to trap melt exacerbates the problem, probably because of early separation of disequilibrium melt.

(2) In general, the determination of melt compositions from peridotite requires a reversal step in which the estimated or analysed melt composition is tested for liquidus temperature and liquidus phases matching those of the forward melting experiment on the peridotite composition. Because of peritectic or incongruent melting relations in peridotite mineralogy, this approach is best achieved by a sandwich or layered experiment in which a layer of the putative melt is equilibrated with a layer of the source peridotite. The product at temperatures near the liquidus of the putative melt layer is an experiment with a melt layer or large melt pool, free of quench modification, and equilibrated with residual mineralogy of the peridotite.

(3) Existing parameterized mantle melting models, whether empirical from experimental data sets or methods combining some thermodynamic constraints together with the experimental data sets, are not in good agreement and do not reproduce 1–2 GPa data presented herein. A necessary first step for such models is the assembly of high-quality experimental data on a well-chosen mix of end-member (simple system) studies and complex, natural rock composition.

ACKNOWLEDGEMENTS

We acknowledge the technical assistance of Keith Harris, Wieslav Jablonski, Nick Ware, Bill Hibberson, and Drs David Steele and Wayne Taylor. Trevor Falloon and Leonid Danyushevsky acknowledge support from the Australian Research Council. We also thank Drs Yaoling Niu, Andy Robinson, Bernie Wood and Ro Kinzler for discussions on mantle melting. We acknowledge support of the Museum of Natural History, Washington, DC, which provided electron microprobe standards.

REFERENCES

Baker, M. B. & Stolper, E. M. (1994). Determining the compositions of high-pressure melts using diamond aggregates. *Geochimica et Cosmochimica Acta* **58,** 2811–2827.

Baker, M. B., Hirschmann, M. M., Ghiorso, M. S. & Stolper, E. M. (1995). Compositions of near-solidus peridotite melts from experiments and thermodynamic calculations. *Nature* **375,** 308–311.

Bowen, N. L. (1914). The ternary system diopside–forsterite–silica. *American Journal of Science* **38,** 207–264.

Danyushevsky, L. V., Falloon, T. J., Sobolev, A. V., Crawford, A. J., Carroll, M. & Price, R. C. (1993). The H_2O content of basalt glasses from Southwest Pacific back-arc basins. *Earth and Planetary Science Letters* **117,** 347–362.

Doukhan, N., Doukhan, J.-C., Ingrin, J., Jaoul, O. & Raterron, P. (1993). Early partial melting in pyroxenes. *American Mineralogist* **78,** 1246–1256.

Falloon, T. J. & Green, D. H. (1987). Anhydrous partial melting of MORB pyrolite and other peridotite compositions at 10 kbar: implications for the origin of primitive MORB glasses. *Mineralogy and Petrology* **37,** 181–219.

Falloon, T. J. & Green, D. H. (1988). Anhydrous partial melting of peridotite from 8 to 35 kbars and the petrogenesis of MORB. In: Menzies, M. A. & Cox, K. G. (eds) *Oceanic and Continental Lithosphere: Similarities and Differences*. *Journal of Petrology,* special issue 379–414.

Falloon, T. J., Green, D. H., O'Neill, H. St C. & Ballhaus, C. G. (1996). Quest for low-degree mantle melts. *Nature* **381,** 285.

Falloon, T. J., Green, D. H., O'Neill, H. St C. & Hibberson, W. O. (1997). Experimental tests of low degree peridotite partial melt compositions: implications for the nature of anhydrous near-solidus peridotite melts at 1 GPa. *Earth and Planetary Science Letters* **152,** 149–162.

Falloon, T. J., Green, D. H., Hatton, C. J. & Harris, K. L. (1988). Anhydrous partial melting of a fertile and depleted peridotite from 2–30 kb and application to basalt petrogenesis. *Journal of Petrology* **29,** 1257–1282.

Falloon, T. J. & Danyushevsky, L. D. (1999). Melting of depleted mantle at 1·5 GPa and 2·0 GPa under H_2O-undersaturated conditions: implications for the petrogenesis of high-Ca boninites. *Journal of Petrology* (submitted).

Ford, C. E., Russell, D. G., Craven, J. A. & Fisk, M. R. (1983). Olivine–liquid equilibria: temperature, pressure and composition dependence of the crystal/liquid cation partition coefficients for Mg, Fe^{2+}, Ca and Mn. *Journal of Petrology* **24,** 256–265.

Frey, F. A., Green, D. H. & Roy, S. D. (1978). Integrated models of basalt petrogenesis—a study of quartz tholeiites to olivine melilitites from southeastern Australia utilizing geochemical and experimental petrological data. *Journal of Petrology* **19,** 463–513.

Fujii, T. & Scarfe, C. M. (1985). Compositions of liquids coexisting with spinel lherzolite at 10 kbar and the genesis of MORBs. *Earth and Planetary Science Letters* **90,** 18–28.

Ghiorso, M. S. & Sack, R. O. (1995). Chemical mass transfer in magmatic processes IV. A revised and internally consistent thermodynamic model for the interpolation and extrapolation of liquid–solid equilibria in magmatic systems at elevated temperatures and pressures. *Contributions to Mineralogy and Petrology* **119,** 197–212.

Green, D. H. & Falloon, T. J. (1998). Pyrolite: a Ringwood concept and its current expression. In: Jackson, I. (ed.) *The Earth's Mantle: Composition, Structure, and Evolution*. Cambridge: Cambridge University Press, pp. 311–378.

Green, D. H. & Ringwood, A. E. (1967). The genesis of basaltic magmas. *Contributions to Mineralogy and Petrology* **15,** 103–190.

Hirschmann, M. M., Baker, M. B. & Stolper, E. M. (1998). The effect of alkalis on the silica content of mantle-derived melts. *Geochimica et Cosmochimica Acta* **62,** 883–902.

Hirose, K. & Kushiro, I. (1993). Partial melting of dry peridotites at high pressures: determination of compositions of melts segregated from peridotites using aggregates of diamonds. *Earth and Planetary Science Letters* **114,** 477–489.

Holloway, J. R. & Wood, B. J. (1988). *Simulating the Earth: Experimental Geochemistry*. London: Unwin & Hyman.

Jaques, A. L. & Green, D. H. (1979). Determination of liquid compositions in high-pressure melting of peridotite. *American Mineralogist* **64,** 1312–1321.

Jaques, A. L. & Green, D. H. (1980). Anhydrous melting of peridotite at 0–15 kbar pressure and the genesis of tholeiitic basalts. *Contributions to Mineralogy and Petrology* **73,** 287–310.

Jarosewich, E. J., Nelen, J. A. & Norberg, J. A. (1980). Reference samples for electron microprobe analyses. *Geostandards Newsletter* **4,** 257–258.

Johannes, W., Bell, P. M., Boettcher, A. L., Chipman, D. W., Hays, J. F., Mao, H. K., Newton, R. C. & Seifert, F. (1971). An interlaboratory comparison of piston–cylinder pressure calibration using the albite-breakdown reaction. *Contributions to Mineralogy and Petrology* **32,** 24–38.

Johnson, K. T. & Kushiro, I. (1992). Segregation of high-pressure partial melts from peridotite using aggregates of diamonds: a new experimental approach. *Geophysical Research Letters* **19,** 1703–1706.

Kinzler, R. J. (1997). Melting of mantle peridotite at pressures approaching the spinel to garnet transition: application to mid-ocean ridge basalt petrogenesis. *Journal of Geophysical Research* **102,** 853–874.

Kinzler, R. J. & Grove, T. L. (1992). Primary magmas of mid-ocean ridge basalts 1. Experiments and methods. *Journal of Geophysical Research* **97,** 6907–6926.

Kushiro, I. (1996). Partial melting of a fertile mantle peridotite at high pressures: an experimental study using aggregates of diamond. In: Basu, A. & Hart, S. R. (eds) *Earth Processes: Reading the Isotopic Code*. Washington, DC: American Geophysical Union, pp. 109–122.

Langmuir, C. H., Klein, E. M. & Plank, T. (1992). Petrological systematics of mid-ocean ridge basalts: constraints on melt generation beneath ocean ridges. In: Morgan, J. P., Blackman, D. K. & Sinton, J. M. (eds) *Mantle Flow and Melt Generation at Mid-ocean Ridges*. Washington, DC: American Geophysical Union, pp. 183–280.

McKenzie, D. & Bickle, M. J. (1988). The volume and composition of melt generated by extension of the lithosphere. *Journal of Petrology* **29,** 625–679.

Myers, J. D. & Johnston, A. D. (1996). Phase equilibria constraints on models of subduction zone magmatism. *American Geophysical Union Monograph* **96,** 229–249.

Niu, Y. (1997). Mantle melting and melt extraction processes beneath ocean ridges: evidence from abyssal peridotites. *Journal of Petrology* **38,** 1047–1074.

Niu, Y. & Batiza, R. (1991). An empirical method for calculating melt compositions produced beneath mid-ocean ridges: application for axis and off-axis (seamount) melting. *Journal of Geophysical Research* **96,** 21753–21777.

O'Hara, M. J. (1968). The bearing of phase equilibrium studies in synthetic and natural systems on the origin and evolution of basic and ultrabasic rocks. *Earth-Science Reviews* **4,** 69–134.

Robinson, J. A. C., Wood, B. J. & Blundy, J. D. (1998). The beginning of melting of fertile and depleted peridotite at 1·5 GPa. *Earth and Planetary Science Letters* **155,** 97–111.

Shen, Y. & Forsyth, D. W. (1995). Geochemical constraints on initial and final depth of melting beneath mid-ocean ridges. *Journal of Geophysical Research* **100,** 2211–2237.

Soulard, H. & Wood, B. J. (1994). Lherzolite partial melting: closer to primary liquids. *Mineralogical Magazine* **58A,** 866–867.

Stolper, E. (1980). A phase diagram for mid-ocean ridge basalts: preliminary results and implications for petrogenesis. *Contributions to Mineralogy and Petrology* **74,** 13–27.

Takahashi, E. (1986). Melting of a dry peridotite KLB-1 up to 14 GPa: implications on the origin of peridotitic upper mantle. *Journal of Geophysical Research* **91,** 9367–9382.

Takahashi, E. & Kushiro, I. (1983). Melting of a dry peridotite at high pressures and basalt magma genesis. *American Mineralogist* **68,** 859–879.

Takahashi, E., Shimazaki, Y., Tsuzaki, Y. & Yoshida, H. (1993). Melting study of a peridotite KLB-1 to 6·5 GPa and the origin of basaltic magmas. *Philosophical Transactions of the Royal Society of London, Series A* **342,** 105–120.

Walter, M. J. & Presnall, D. C. (1994). Melting behaviour of simplified lherzolite in the system $CaO–MgO–Al_2O_3–SiO_2–Na_2O$ from 7 to 35 kbar. *Journal of Petrology* **35,** 329–359.